JACS
JOURNAL OF THE AMERICAN CHEMICAL SOCIETY
Article
pubs.acs.org/JACS
Terms of Use

Ultra-pH-Sensitive Nanoprobe Library with Broad pH Tunability and Fluorescence Emissions

Xinpeng Ma,[†,‡] Yiguang Wang,[†,‡] Tian Zhao,[†] Yang Li,[†] Lee-Chun Su,[†] Zhaohui Wang,[†] Gang Huang,[†] Baran D. Sumer,[§] and Jinming Gao*[,†,∥]

[†]Department of Pharmacology and [§]Department of Otolaryngology, Simmons Comprehensive Cancer Center, University of Texas Southwestern Medical Center, Dallas, Texas 75390, United States

[∥]Department of Chemistry, University of Texas at Dallas, Richardson, Texas 75083, United States

Supporting Information

ABSTRACT: pH is an important physiological parameter that plays a critical role in cellular and tissue homeostasis. Conventional small molecular pH sensors (e.g., fluorescein, Lysosensor) are limited by broad pH response and restricted fluorescent emissions. Previously, we reported the development of ultra-pH-sensitive (UPS) nanoprobes with sharp pH response using fluorophores with small Stokes shifts (<40 nm). In this study, we expand the UPS design to a library of nanoprobes with operator-predetermined pH transitions and wide fluorescent emissions (400−820 nm). A copolymer strategy was employed to fine tune the hydrophobicity of the ionizable hydrophobic block, which led to a desired transition pH based on standard curves. Interestingly, matching the hydrophobicity of the monomers was critical to achieve a sharp pH transition. To overcome the fluorophore limitations, we introduced copolymers conjugated with fluorescence quenchers (FQs). In the micelle state, the FQs effectively suppressed the emission of fluorophores regardless of their Stokes shifts and further increased the fluorescence activation ratios. As a proof of concept, we generated a library of 10 nanoprobes each encoded with a unique fluorophore. The nanoprobes cover the entire physiologic range of pH (4−7.4) with 0.3 pH increments. Each nanoprobe maintained a sharp pH transition (on/off < 0.25 pH) and high fluorescence activation ratio (>50-fold between on and off states). The UPS library provides a useful toolkit to study pH regulation in many pathophysiological indications (e.g., cancer, lysosome catabolism) as well as establishing tumor-activatable systems for cancer imaging and drug delivery.

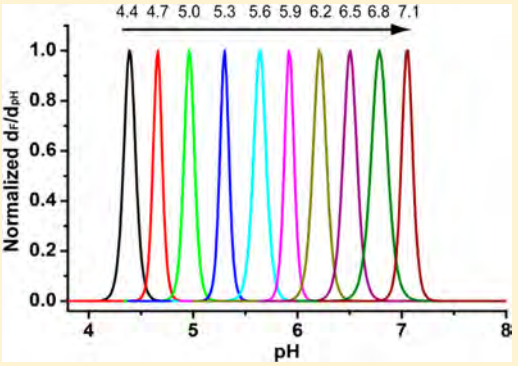

INTRODUCTION

Nanomaterials responsive to external stimuli such as pH, temperature, reactive oxygen/nitrogen species, or enzyme levels have been extensively explored for a wide range of biological applications in molecular sensing, drug delivery, and tissue engineering.[1−5] Compared to small molecular sensors, responsive nanomaterials often display positive cooperativity with sharpened responses, a hallmark of the supramolecular self-assembly system described by Whitesides over two decades ago.[6,7] Supramolecular self-assembly engages a multitude of multivalent, weak, and reversible noncovalent interactions (e.g., electrostatic, hydrogen bonding, and hydrophobic interactions) to form thermodynamically stable nanostructures ($\Delta G \leq 0$). This strategy has the advantage of dramatic phase transitions upon subtle perturbation of environmental stimuli. Such strategies have been exploited in artificial systems such as thermosensitive hydrogels (e.g., NIPAM,[8] elastin-like proteins[9]) for drug delivery, as well as by nature in protein oligomerization to counter large-scale cellular responses to amplify biological signals.[10]

In recent years, our lab has focused on the development of ultra-pH-sensitive (UPS) nanoparticles using self-assembly principles. pH is an important physiological signal that plays a critical role in maintaining cellular and tissue homeostasis. At the molecular level, the pH gradient across the mitochondria membrane is essential for ATP synthesis.[11] At the cellular level, the pH of intracellular compartments (e.g., endocytic vesicles) in eukaryotic cells is carefully controlled and directly affects many processes such as membrane transport, receptor cycling, lysosomal catabolism, and virus entry into cells.[12−14] Inhibition of lysosomal function by the impairment of lysosomal pH has been associated with the lack of Aβ degradation and subsequent neuronal cell death in Alzheimer's disease.[15,16] At the tissue level, the interstitial pH is carefully controlled at 7.2−7.4. In the tumor microenvironment, cancer cells display a "reversed" pH gradient with a constitutively increased cytoplasmic pH and lowered extracellular pH (pH_e = 6.5−6.9)[17,18] that promotes matrix degradation and cancer metastasis. Recently, this dysregulated pH has been described as a universal characteristic of cancer.[17]

Received: May 27, 2014
Published: July 14, 2014

   dx.doi.org/10.1021/ja5053158 | J. Am. Chem. Soc. 2014, 136, 11085−11092

Previously, we reported a series of ultra-pH-sensitive micelle nanoparticles using a block copolymer design (PEO-*b*-PR, where PEO is poly(ethylene oxide) and PR is an ionizable tertiary amine block).[19−22] Tertiary amine-containing monomers with precisely controlled hydrophobic substituents were employed to render different pH transitions. At low pH, micelles dissociate into cationic unimers with protonated ammonium groups (left panel in Figure 1a). Fluorophores conjugated on the PR segment emit strong fluorescence. When pH increases, the neutralized PR segments become hydrophobic and self-assemble into the micelles, which results in fluorescence quenching (right panel). Hydrophobic micellization dramatically sharpens the pH transitions (on/off states is <0.25 pH unit, compared to 2 pH units for small molecular pH sensors as dictated by the Henderson−Hasselbalch equation[23]). Using this design, we successfully differentiated the compartmental pH between early endosomes (6.0−6.5) and late endosomes/lysosomes (4.5−5.5), which led to an early endosome-activatable nanocarrier (transition pH, or pH_t = 6.3) for siRNA delivery.[24] More recently, we demonstrated the use of a pH_t 6.9 nanoprobe to turn on the fluorescence signal in the acidic microenvironment of tumors (pH_e = 6.5−6.9) while keeping silent during blood circulation (7.4) for cancer-specific imaging of a broad range of tumors.[22]

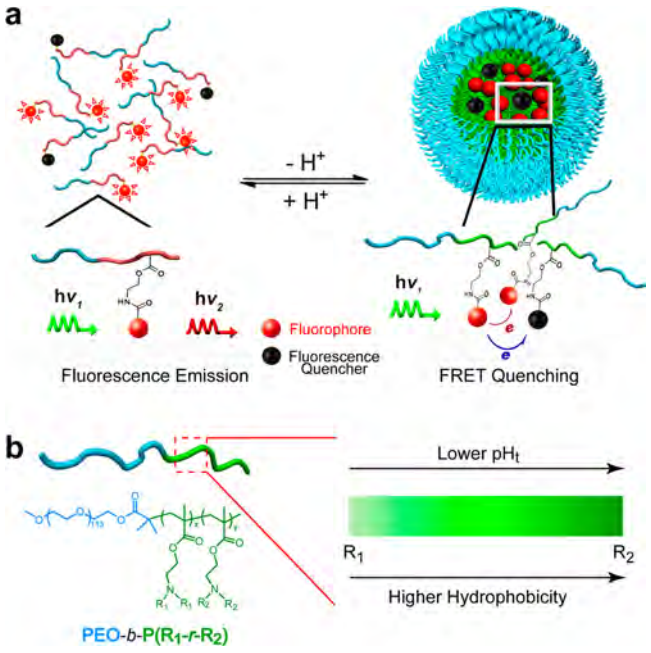

Figure 1. Schematic design of ultra-pH-sensitive (UPS) micellar nanoprobes. (a) In the unimer state (pH < pH_t), polymer dissociation resulted in fluorophore/quencher separation and strong fluorescence emission. In the micelle state (pH > pH_t), fluorescence quenching dramatically suppresses the emission intensity of fluorophores. (b) A random copolymer strategy was used to achieve an operator-predetermined control of nanoprobe pH_t by the ability to continuously fine tune the hydrophobicity of the PR segment.

Despite these successes, the previous UPS nanoprobe design is limited in two aspects: first, the homopolymeric PR segment synthesized from a single monomer only provides limited control of transition pH; second, the fluorophores were limited to those with a small Stokes shift (<40 nm) due to the homoFRET-induced decay mechanism. To overcome these limitations, we now report a copolymer strategy to fine tune the hydrophobicity of the PR segment for pH_t control (Figure 1b) and, moreover, to introduce fluorescence quenchers (FQs) to broaden the dye selection. Consequently, we established a UPS library with operator-predetermined pH transitions covering the entire physiologic pH range from 4 to 7.4 using a wide range of fluorophores (400−820 nm). The library consists of 10 nanoprobes with 0.3 pH increment each encoded with a unique fluorophore. Each nanoprobe maintained the sharp pH transition (on/off < 0.25 pH) and high fluorescence activation ratio (>50-fold between on and off states). This UPS library provides a valuable toolkit to interrogate a variety of cell physiological processes involving pH regulation as well as tumor-activatable systems for image-guided surgery and drug delivery applications.

RESULTS AND DISCUSSION

Copolymer Syntheses by the ATRP Method. We used the atom transfer radical polymerization (ATRP) method[25,26]

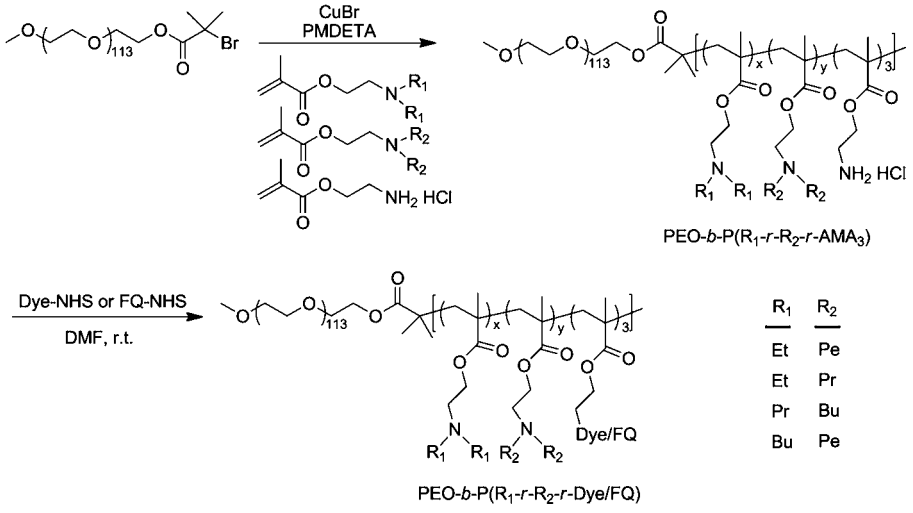

Figure 2. Syntheses of dye- or fluorescence quencher (FQ)-conjugated PEO-*b*-P(R_1-*r*-R_2) copolymers. The hydrophobicity of the PR segment can be continuously controlled by varying the molar fractions of the two monomers (R_1 or R_2 = Et, ethyl; Pr, propyl; Bu, butyl; Pe, pentyl).

dx.doi.org/10.1021/ja5053158 | J. Am. Chem. Soc. 2014, 136, 11085−11092

with CuBr as a catalyst and *N*,*N*,*N*′,*N*′,*N*″-pentamethyldiethylenetriamine (PMDETA) ligand for copolymer synthesis (Figure 2). The PEO-*b*-PR copolymers with homopolymeric PR block were synthesized using a single metharylate monomer as previously described.[19,20] In order to continuously fine tune the hydrophobicity of the PR segment, we employed a copolymerization strategy using two methacrylate monomers with different hydrophobicity (Figure 2). The molar fraction of the two monomers can be precisely controlled prior to polymerization, leading to a random copolymerized P(R_1-*r*-R_2) block.[27] A series of methacrylate monomers with different dialkyl chain lengths (e.g., ethyl, propyl, butyl, and pentyl) was used in the current study. To introduce fluorophores or fluorescence quenchers, we also incorporated aminoethyl methacrylate (AMA-MA) (three repeating units per polymer chain) where the free amino groups were conjugated to dyes or FQs through activated *N*-hydroxyl succinimidyl (NHS) esters.

After syntheses, we characterized the copolymers with ^{1}H and ^{13}C NMR to verify the chemical composition and used gel permeation chromatography (GPC) to measure the number- and weight-averaged molecular weights and polydispersity (Supporting Information Tables S1−S3, Figures S1−S6). GPC analysis of representative dye-conjugated copolymers showed complete removal of the free dyes after purification (Supporting Information Figure S7). Glass transition temperatures (T_g) and melting temperatures (T_m) of the copolymers were measured by differential scanning calorimetry (DSC). The onset decomposition temperatures (T_d) and temperature of 50% weight loss (T_{50}) were measured by thermogravimetric analysis (TGA, Supporting Information Tables S3). The apparent pK_a values of the copolymers were obtained by pH titration (Supporting Information Tables S1, S2, and S4).

Comparison of Copolymerization vs Molecular Mixture Strategy for pH$_t$ Control. Initially, we compared two different strategies on their abilities to control the pH$_t$ values of UPS nanoprobes. The first strategy involves a molecular mixture of two different PEO-*b*-PR copolymers with different pH transitions. In this example, we used Cy5-conjugated PEO-*b*-poly[2-(diethylamino)ethyl methacrylate] (**PDEA**, all copolymers were conjugated with Cy5 dye in the PR segment unless specified otherwise) and PEO-*b*-poly[2-(dipentylamino)ethyl methacrylate] (**PD5A**). The **PDEA** and **PD5A** nanoprobes had pH transitions at 4.4 and 7.8, respectively. We used a sonication method to produce a micelle nanoprobe consisting of both copolymers with the same molar percentage (i.e., 50%) in each micelle (this was verified by heteroFRET experiments, data not shown). In the second strategy, we synthesized the Cy5-conjugated PEO-*b*-poly[2-(diethylamino)ethyl methacrylate-*r*-2-(dipentylamino)ethyl methacrylate] copolymer (**P(DEA$_{40}$-D5A$_{40}$)**; unless noted otherwise, this nomenclature (without r) refers to a random PR block) where the PR segment was composed of a random copolymer from two monomers (40 repeating units for each monomer, Supporting Information Table S1). The hydrodynamic diameters were 65 and 29 nm for **PDEA/PD5A** (molecular mixture) and **P(DEA$_{40}$-D5A$_{40}$)** (copolymer) micelles, respectively.

The two micelle designs show drastically different patterns of fluorescence emission in response to changes in pH. For the **PDEA/PD5A** nanoprobes, we observed two distinctive pH transitions corresponding to the individual copolymers where the fluorescence on/off transitions were at 4.4 and 7.8 (Figure 3a, Supporting Information Figure S8). This result suggests that

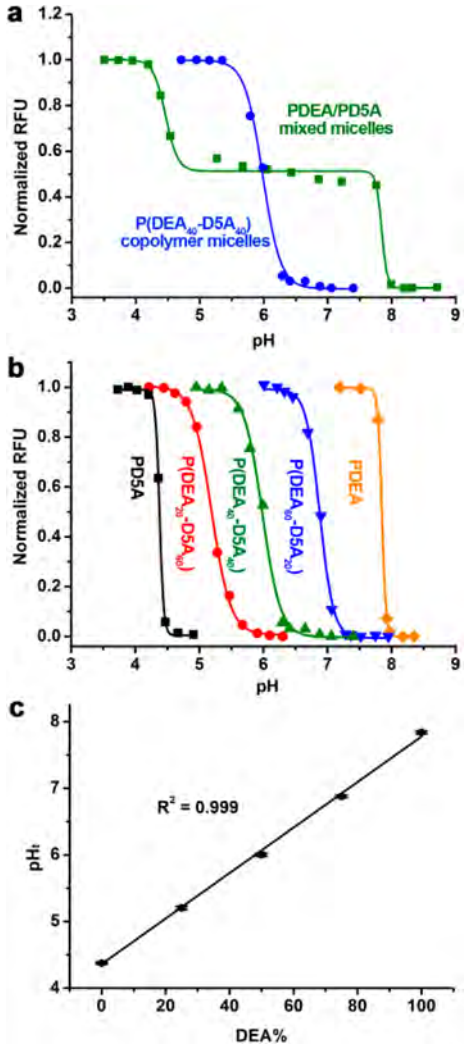

Figure 3. (a) Comparison of **PDEA/PD5A** molecular mixture vs **P(DEA$_{40}$-D5A$_{40}$)** copolymer strategies for control of pH$_t$. (b) Normalized fluorescence intensity of **P(DEA$_x$-D5A$_y$)** nanoprobes with different ratios of the two monomers as a function of pH. (c) Nanoprobe pH$_t$ is linearly correlated with the molar fraction of the DEA-MA monomer in the PR segment. Error bars were calculated from three repeating experiments (n = 3). Polymer concentrations were 0.1 mg/mL in these studies.

chain entanglement between PDEA and PD5A within the micelle core is not sufficient to overcome individual polymer dissociation behavior. In contrast, the **P(DEA$_{40}$-D5A$_{40}$)** nanoprobe showed a single pH transition at 6.0, about halfway between the **PDEA** and the **PD5A** transitions.

To explore the control of transition pH, we synthesized a series of **P(DEA$_x$-D5A$_y$)** copolymers with varying molar fractions of the two monomers. The resulting copolymers displayed different pH transitions (Figure 3b, Supporting Information Figure S9). Plot of pH$_t$ of nanoprobes as a function of the molar fraction of DEA monomer showed a linear correlation (Figure 3c). Incorporation of a higher percentage of less hydrophobic monomers (e.g., DEA-MA) resulted in higher pH transitions. It is worth pointing out that the transition pH of the UPS nanoprobes is controlled by varying the hydrophobicity of the PR segment. This is contrary to small molecular pH sensors, where electron-withdrawing or -donating groups are necessary for fine tuning.[28]

dx.doi.org/10.1021/ja5053158 | J. Am. Chem. Soc. 2014, 136, 11085−11092

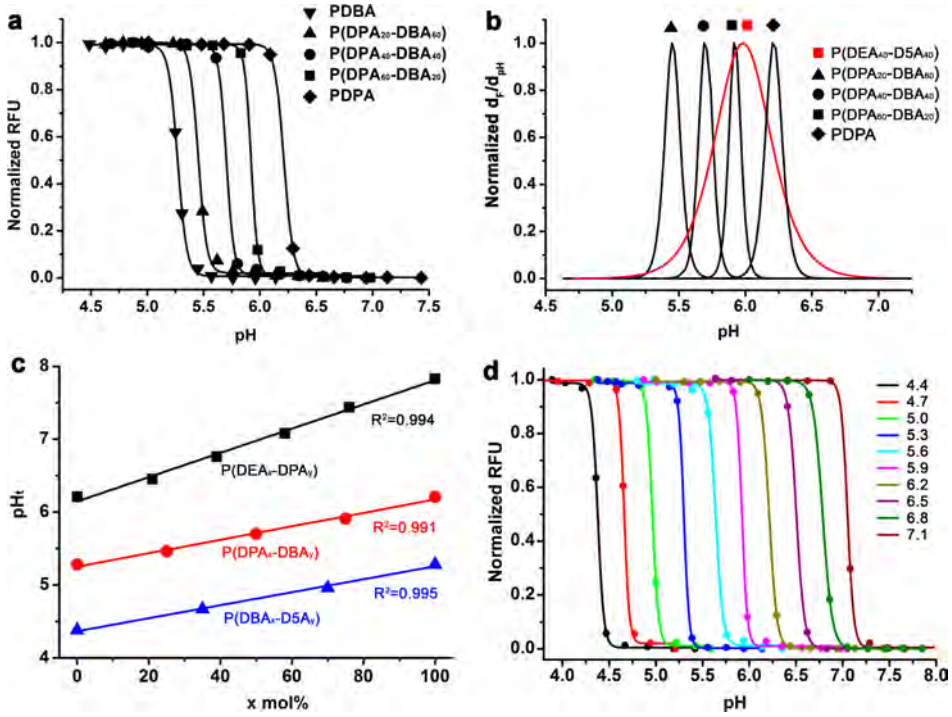

Figure 4. (a) Normalized fluorescence intensity as a function of pH for Cy5-conjugated **P(DPA$_x$-DBA$_y$)** nanoprobes. (b) Derivative fluorescence plot (d_F/d_{pH}, data from a) as a function of pH for **P(DPA$_x$-DBA$_y$)** vs **P(DEA$_{40}$-D5A$_{40}$)** nanoprobes. Use of methacrylate monomers with close hydrophobicity (i.e., DPA/DBA vs DEA/D5A) resulted in much sharper pH transitions. (c) Linear relationships of the nanoprobe pH_t vs molar fraction of the less hydrophobic monomer for different copolymer compositions. These correlations serve as the standard curves for selecting the optimal copolymer composition to achieve an operator-predetermined pH_t. (d) Representative library of UPS nanoprobes with 0.3 pH increment covering the physiologic range of pH 4–7.4. All nanoprobes were conjugated with the Cy5 dye. Polymer concentrations were at 0.1 mg/mL.

Monomer Compatibility Affects Sharpness of pH Transition. Although **P(DEA$_x$-D5A$_y$)** nanoprobes with different monomer percentage allowed control of transition pH (Figure 3b and 3c), the sharpness of the pH transition was significantly broader than the corresponding nanoprobes with homopolymeric PR segment. More specifically, the $\Delta pH_{10-90\%}$ values (pH range where fluorescence intensity increases from 10% to 90%) were 0.65, 0.64, and 0.47 for **P(DEA$_x$-D5A$_y$)** copolymers with 25%, 50%, and 75% of DEA-MA compositions, respectively, in comparison to 0.14 and 0.19 for **PDEA** and **PD5A** nanoprobes, respectively. The broad pH response from **P(DEA$_x$-D5A$_y$)** copolymers indicates the heterogeneous chain properties from the monomers with large hydrophobicity differences.

To improve the sharpness of pH transition, we investigated the use of monomers with closely matched hydrophobicity. As an example, we chose 2-(dipropylamino)ethyl methacrylate (DPA-MA) and 2-(dibutylamino)ethyl methacrylate (DBA-MA) to produce a series of **P(DPA$_x$-DBA$_y$)** nanoprobes. The two monomers differ by one carbon on the nitrogen substituents (i.e., propyl vs butyl). Copolymerization of the two monomers led to a more refined, tunable series of nanoprobes with sharp pH transitions (Figure 4a, Supporting Information Figure S10). The $\Delta pH_{10-90\%}$ values were 0.19, 0.20, and 0.18 for **P(DPA$_x$-DBA$_y$)** nanoprobes with 25%, 50%, and 75% of DPA-MA compositions, respectively. Each copolymer probe maintained the sharp pH transition (<0.25 pH unit). Figure 4b shows a fluorescence derivative plot as a function of pH, which further illustrates the greatly increased sharpness of serial **P(DPA$_x$-DBA$_y$)** nanoprobes compared to a single **P(DEA$_{40}$-D5A$_{40}$)** nanoprobe in the same pH span.

To further investigate the PR structure on nanoprobe performance, we also synthesized two Cy5-conjugated triblock copolymers, **PEO-*b*-P(D5A$_{40}$-*b*-DEA$_{40}$)** and **PEO-*b*-P(DBA$_{40}$-*b*-DPA$_{40}$)** (or **P(D5A$_{40}$-*b*-DEA$_{40}$)** and **P(DBA$_{40}$-*b*-DPA$_{40}$)**, where b is used to denote the diblock nature of the PR_1 and PR_2 segments). pH titration experiments showed two distinctive ionization transitions for the **P(D5A$_{40}$-*b*-DEA$_{40}$)** and **P(DBA$_{40}$-*b*-DPA$_{40}$)** copolymers (Supporting Information Figures S11a and S11c). In contrast, only one pH transition was observed for the corresponding random PR block copolymers. For the **P(D5A$_{40}$-*b*-DEA$_{40}$)** nanoprobe, we observed two fluorescence transitions at pH 5.3 and 6.1 (Supporting Information Figure S11b), which is attributed to $D5A_{40}$ and DEA_{40} blocks, respectively. For the **P(DBA$_{40}$-*b*-DPA$_{40}$)** nanoprobe, we were not able to detect two distinctive fluorescence transitions over pH (Supporting Information Figure S11d). However, the pH response for this probe ($\Delta pH_{10-90\%}$ = 0.64) is considerably broader than the **P(DPA$_{40}$-*r*-DBA$_{40}$)** nanoprobe ($\Delta pH_{10-90\%}$ = 0.20). It is interesting to note that the pH_t values of the two nanoprobes were also different (5.51 vs 5.70 for the **P(DBA$_{40}$-*b*-DPA$_{40}$)** and **P(DBA$_{40}$-*r*-DPA$_{40}$)** nanoprobes, respectively) despite similar chemical compositions. These results indicate that in addition to chemical composition, PR architecture also affects the physicochemical and fluorescence properties of the resulting nanoprobes. On the basis of these data, we conclude that a random copolymer (i.e., $P(R_1\text{-}r\text{-}R_2)$) from monomers with closely matched hydrophobicity provides the best strategy to fine tune the hydrophobicity of PR block to achieve a single and sharp pH transition for construction of UPS library.

dx.doi.org/10.1021/ja5053158 | J. Am. Chem. Soc. 2014, 136, 11085–11092

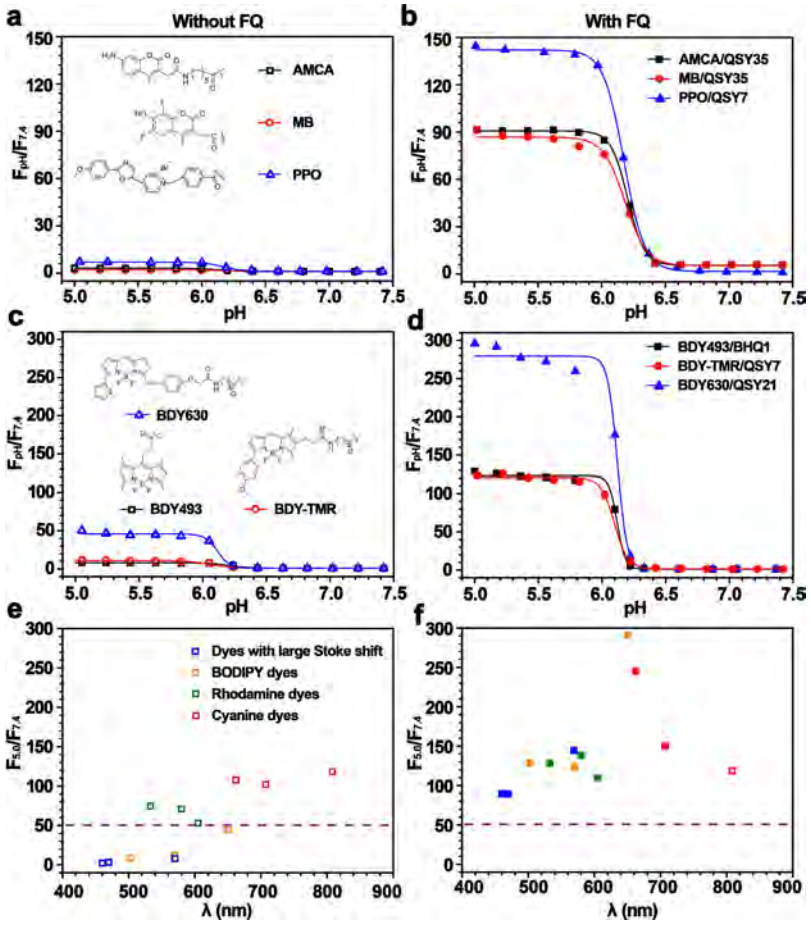

Figure 5. Introduction of FQ-conjugated **PDPA** copolymer significantly increased the fluorescence activation ratio of different **PDPA-dye** nanoprobes. Fluorescence intensity ratio at different pH to pH 7.4 ($F_{pH}/F_{7.4}$) was plotted for copolymer alone (a, c, and e) and with addition of FQ-conjugated copolymers (b, d, f). See main text for detailed description and Supporting Information Figure S19 for the structures of the dyes and FQs.

A plot of pH_t values of the **P(DPA$_x$-DBA$_y$)** nanoprobes as a function of the molar fraction of DPA-MA monomer yielded a linear correlation (Figure 4c). Similarly, we established standard curves for **P(DBA$_x$-D5A$_y$)** and **P(DEA$_x$-DPA$_y$)** series. These standard curves allow for rational design of UPS nanoprobes with any predetermined pH transitions (between 4.4 and 7.8) by choosing copolymers with correct PR compositions (i.e., monomer pairs and molar fractions). For proof of concept, we generated a UPS library consisting of 10 nanoprobes at 0.3 pH increment covering the entire physiologic range of pH (4−7.4) with each nanoprobe maintaining the sharp pH transition (<0.25 pH unit between on and off states, Figure 4d, Supporting Information Figures S12 and S13). Particle size and size distribution, zeta potential at pH 7.4 in the PBS buffer, and corresponding pK_a and pH_t values for each nanoprobe are listed in the Supporting Information Table S4.

To verify the pH-dependent micelle assembly of the copolymer nanoprobes, we chose two representative samples, **P(DEA$_{40}$-D5A$_{40}$)** and **P(DPA$_{40}$-DBA$_{40}$)**, and employed dynamic light scattering (DLS) and transmission electron microscopy (TEM) to study these samples at pH above and below their pH_t (5.99 and 5.70, respectively). At pH 7.4 in the PBS buffer, both nanoprobes were present as spherical micelles by TEM and the hydrodynamic diameters (D_h) were 29.4 ± 3.4 and 36.3 ± 2.4 nm for **P(DEA$_{40}$-D5A$_{40}$)** and **P(DPA$_{40}$-DBA$_{40}$)** by DLS analysis, respectively (Supporting Information Figures S14 and S15, Table S5). At pH 5.0, both micelles dissociated into unimers with decrease of D_h to 9.2 ± 0.4 and 7.3 ± 0.7 nm, respectively. TEM and DLS analyses of both nanoprobes in 10% fetal bovine serum (FBS) in cell culture medium showed similar pH dependence, suggesting the stability of the nanoprobes in the biological environment at pH 7.4. Additional stability study using TMR-conjugated UPS$_{6.5}$ nanoprobe (**P(DEA$_{21}$-DPA$_{79}$)**) showed a high fluorescence activation ratio (>40-fold) in the presence of 10% FBS, 50% mouse serum, or solutions containing different serum proteins (e.g., 20 mg/mL albumin, 5 mg/mL γ-globulin) at 37 °C over 24 h (Supporting Information Figure S16).

Characterization of Dye-Conjugated Copolymers. In the copolymer syntheses (Figure 2), we introduced three primary amine-containing AMA-MA units per polymer chain. In this study, we chose four representative NHS esters of marina blue (MB), BDY493, TMR, and Cy5 and conjugated them to a model **PDPA** copolymer. After purification of free dyes from the dye-conjugated copolymer, we measured the yields of dye conjugation and studied the photophysical properties of the resulting nanoprobes. Results show consistent 68−72% conjugation efficiency for these fluorophores, which corresponds to an average of two dyes per polymer chain (Supporting Information Table S6). To investigate the photophysical properties, we measured the quantum yields (Φ_F) of polymer-conjugated dyes and compared them to the

dx.doi.org/10.1021/ja5053158 | J. Am. Chem. Soc. 2014, 136, 11085−11092

free dyes in methanol. As a control, we also measured the quantum yields of free dyes in a physical mixture with the same quantity of dye-free copolymers. Results show the quantum yields of polymer-conjugated dye did not change for Cy5 (Φ_F = 0.28), decreased to a small degree for MB (0.89 to 0.73), and decreased greatly for TMR (from 0.68 to 0.15 from free TMR to polymer-conjugated TMR, respectively). The large decrease of Φ_F for TMR can be due to formation of H-dimers as previously reported.[20] Interestingly, the Φ_F value decreased dramatically from 0.90 of free BDY493 to 0.10 for polymer-conjugated BDY493. Addition of a small amount of HCl in methanol solution recovered the Φ_F to 0.87, suggesting that photoinduced electron transfer (PeT) from free tertiary amines (before protonation) to BDY493 is responsible for fluorescence quenching. Intramolecular PeT yielded much more efficient quenching since a physical mixture of dye-free polymer at the same polymer concentration only slightly decreased the Φ_F of the free dye (0.86, Supporting Information Table S6).

We formed micelle nanoprobes from **PDPA-TMR** and **PDPA-BDY493** copolymers (pH_t = 6.2) and measured the Φ_F values at the micelle state (pH 7.4) and unimer state (pH 5.0) in aqueous environment. For the **PDPA-TMR** nanoprobe, the Φ_F value decreased from 0.25 at pH 5.0 to 0.0048 at pH 7.4, representing a 52-fold decrease from the on to off state of the nanoprobe. In contrast, the Φ_F value of **PDPA-BDY493** decreased only 12-fold from pH 5.0 (Φ_F = 0.93) to pH 7.4 (0.076). Cell culture experiments using the **PDPA-BDY493** and **PDPA-MB** nanoprobes showed high medium background signal and low imaging contrast of H2009 cancer cells (SNR_{cell}/SNR_{Med} < 5, where SNR_{cell} and SNR_{Med} are the signal-to-noise ratios of the cancer cells and medium, respectively, Supporting Information Figures S17 and S18). A better nanoprobe design with large fluorescence activation ratio between the off and on states is necessary to improve cellular imaging specificity.

Use of Fluorescence Quenchers To Broaden Fluorophore Selection. Previously, we reported homo-FRET-induced fluorescence decay as the main mechanism to achieve the on/off activatable design of the UPS nanoprobes.[20] This mechanism only applies to fluorophores (e.g., rhodamine and cyanine dyes) with small Stokes shifts (<40 nm). For dyes with large Stokes shifts (e.g., marina blue or PPO, $\Delta\lambda \geq 100$ nm), the fluorescence activation ratio ($R_F = F_{on}/F_{off}$, where F_{on} and F_{off} are the fluorescence intensity at on and off states, respectively) was less than 5. Moreover, for BODIPY dyes, the fluorescence activation ratio is relatively low (R_F <15) as a result of the PeT mechanism.[29−31]

To overcome these limitations, we investigated the use of fluorescence quenchers (FQs) to broaden the fluorophore selection. Fluorescence quenchers have been widely used by many groups for the design of activatable imaging probes.[32−35] The mechanism is based on the fluorescence resonance energy transfer from desired fluorophores to the FQs, which subsequently dissipate the radiative energy into heat. In this design, we selected a series of FQs that are sensitive to different emission wavelengths and conjugated them onto the copolymer. The UPS nanoprobes were produced by mixing the FQ-conjugated polymer with dye-conjugated polymer in the same micelle core. At the micelle state, FQs quench the fluorophore signals, and upon micelle dissociation, separation of FQs and fluorophores will result in a significant increase in fluorescence emissions (Figure 1a).

To evaluate the effectiveness of the FQ strategy, we used PEO-*b*-poly[2-(propylamino)ethyl methacrylate] (**PDPA**) as a model system and conjugated different FQs and fluorophores to the copolymer (Supporting Information Figure S19). The **PDPA** nanoprobe had a pH transition at 6.2. First, we investigated the FQ strategy on fluorophores with large Stokes shift (e.g., AMCA, 353/442; MB, 362/462; PPO, 415/570; the two numbers refer to the excitation and emission wavelengths, respectively). Without introduction of FQ-conjugated polymer, the **PDPA-AMCA** and **PDPA-MB** nanoprobes showed only 3-fold fluorescence activation between the on and the off states at pH 5.0 and 7.4, respectively (Figure 5a). Introduction of **PDPA-QSY35** to **PDPA-AMCA** or **PDPA-MB** resulted in a significant increase in fluorescence activation, which reached a plateau when the molar fraction of **PDPA-QSY35** became 67% (Supporting Information Figure S20). At this composition, the R_F values reached approximately 90-fold, which are 30 times higher than those without the FQs (Figure 5b, Supporting Information Figure S21). Similarly, introduction of **PDPA-QSY7** (50 mol %) to **PDPA−PPO** nanoprobes increased the R_F value from 6 to >130-fold, respectively (Figure 5b).

For the BODIPY family of dyes, the **PDPA-BDY493** and **PDPA-TMR** nanoprobes only yielded a ∼15-fold increase of fluorescence upon activation (Figure 5c), which is not adequate for biological applications (e.g., during cellular imaging, an R_F value >30 is necessary to suppress the background signal). Introduction of **PDPA-BHQ1** (50 mol %) and **PDPA-QSY7** (50 mol %) to the **PDPA-BDY493** and **PDPA-BDYTMR** nanoprobes led to dramatically increased R_F values (both >100-fold, Figure 5d, Supporting Information Figure S22). Interestingly, **PDPA-BDY630** alone was able to achieve a 40-fold R_F value. Addition of **PDPA-QSY21** further increased the R_F value to over 250-fold (Figure 5d).

Previous studies showed that rhodamine and cyanine dyes with small Stokes shifts (<40 nm) were able to produce UPS nanoprobes with large R_F values through the homoFRET-induced fluorescence decay mechanism.[20] Results from this study confirmed the previous report, where **PDPA-dye** copolymers alone reached >50-fold and >100-fold for rhodamine and cyanine dyes, respectively. Addition of FQ-conjugated copolymer (except Cy7.5 for which there is no FQ) further increased the R_F values for these nanoprobes (Figure 5f, Supporting Information Figures S23−25).

Figure 5e and 5f summarizes the fluorescence activation ratios ($R_F = F_{5.0}/F_{7.4}$) for all fluorophores used in the **PDPA** nanoprobes with and without introduction of fluorescence quenchers. Data show that with addition of FQ-conjugated polymer all fluorophores (12 in total) showed universally high activation ratios (>50-fold) regardless of the Stokes shift or PeT mechanism. In addition, introduction of FQ-conjugated polymer did not affect the sharpness of pH transitions (all composite nanoprobes had <0.25 pH unit between on and off states, Figure 5b and 5d and Supporting Information Figure S25b and S25d).

Cell uptake studies of (**PDPA-MB/PDPA-QSY35**) and (**PDPA-BDY493/PDPA-BHQ1**) nanoprobes showed significantly increased cellular imaging contrast over the medium background. These nanoprobes remained silent in the cell culture medium. Upon uptake in the endosomes/lysosomes in the H2009 lung cancer cells, the nanoprobes were activated by the acidic organelle pH, leading to dramatically increased fluorescence intensity. The SNR_{cell}/SNR_{Med} ratios increased to 29- and 94-fold for (**PDPA-MB/PDPA-QSY35**) and (**PDPA-BDY493/PDPA-BHQ1**) nanoprobes, respectively, much high-

dx.doi.org/10.1021/ja5053158 | J. Am. Chem. Soc. 2014, 136, 11085−11092

er than those without the fluorescence quenchers (Supporting Information Figures S17 and S18).

UPS Library Spanning a Large Range of pH Transitions and Fluorescence Emissions. On the basis of the above results, we produced a representative UPS library consisting of 10 nanoprobes each encoded with a different fluorophore. The composition for each nanoprobe follows that from Figure 4d (see Supporting Information Tables S3 and S4 for details), which resulted in a collection with 0.3 pH increments in the pH span of 4 to 7.4. For each nanoprobe, a series of aqueous solutions of the copolymer at the same polymer concentration (i.e., 0.1 mg/mL) but different pH values was prepared. For **4.4-AMCA**, **4.7-MB**, **5.0-BDY493**, and **6.2-BDY630** nanoprobes, the corresponding copolymers were mixed with the same equivalent of FQ-conjugated matching copolymers to achieve high on/off contrast. Figure 6 shows the emission image of the UPS nanoprobe library at

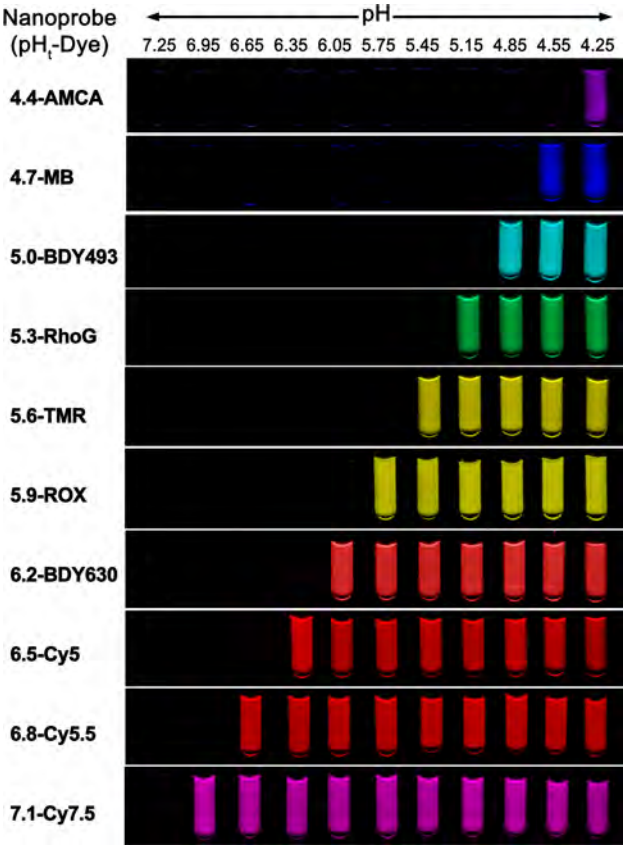

Figure 6. Exemplary UPS library consisting of 10 nanoprobes spanning a wide pH range (4–7.4) and large fluorescent emissions (400–820 nm). Each nanoprobe is encoded by its transition pH and fluorophore. Images of **4.4-AMCA** and **4.7-MB** were taken by a camera at an excitation light of 365 nm. Images of the rest of the nanoprobe solutions were taken on a Maestro Imaging system.

the excitation/emission wavelengths corresponding to each fluorophore. To evaluate the potential toxic effects of the UPS nanoprobes, we performed MTT assay in the H2009 lung cancer cells. H2009 cells were incubated with increasing concentrations (from 0.1 to 100 μg/mL) of different nanoprobes in the cell culture medium for 48 h at 37 °C (typical imaging dose is below 100 μg/mL). Results showed minimal toxicity (cell viability > 90%) for a majority of the nanoprobes (Supporting Information Figure S26). UPS$_{7.1}$ and UPS$_{6.8}$ showed slightly higher toxicity (80% viability) at 100 μg/mL. Current work is in progress to study the pH-dependent perturbation of lysosome catabolism and oncogenic signaling pathway and their impact on cell viability at higher doses (>400 μg/mL) of the UPS nanoparticles.

Results from Figure 6 illustrate the exquisite pH sensitivity of the UPS nanoprobes to the external environment spanning the entire physiologic pH of 4–7.4. In the lowest pH range, the **4.4-AMCA** nanoprobe was off at pH 4.55 but can be turned on at pH 4.25. This nanoprobe can be useful in detection of functional lysosomal pH where hydrolases require a lower pH for enzyme activity. The on/off characteristics of the nanoprobes make them particularly useful in high-throughput screening applications to identify molecular pathways or small molecular perturbators that affect lysosomal function. The nanoprobes covering the higher pH range (e.g., 6.5–7.1) can be useful for differentiation of the acidic pH$_e$ of tumors with different glycolysis rates of the cancer cells.[22,36] The nanoprobes in the intermediate range (e.g., 5.0–6.5) may be useful for study of the maturation of endosomes/lysosomes and to establish organelle-specific compositions for subcellular imaging or drug delivery applications.

CONCLUSIONS

We report a robust method for development of ultra-pH-sensitive (UPS) micellar nanoprobes with significantly improved pH control and broadened fluorophore selection over the previous methods.[19,20] Through a copolymerization strategy for synthesis of the ionizable block, we demonstrate the ability to achieve an operator-predetermined control of the transition pH of the UPS nanoprobes based on standard curves. Importantly, matching of the hydrophobicity of the two monomers is critical to ensure the sharpness of pH transition (i.e., <0.25 pH between the on and the off states). Introduction of fluorescence quenchers in the core of the UPS nanoprobes further broadens the fluorophore choice to those with large Stokes shifts. On the basis of these findings, we established a UPS nanoprobe library consisting of 10 components with 0.3 pH increment that span the entire physiologic range of pH (4–7.4). Each nanoprobe maintained exquisite sensitivity to the environmental pH. The availability of the UPS library opens up many exciting opportunities for basic biological research (e.g., endosome/lysosome biology) as well as for translational studies in tumor imaging and drug delivery.

ASSOCIATED CONTENT

Supporting Information

Materials, methods, detailed experimental procedures (synthesis, characterization, and biological assays), and supplementary figures. This material is available free of charge via the Internet at http://pubs.acs.org.

AUTHOR INFORMATION

Corresponding Author

E-mail: jinming.gao@utsouthwestern.edu

Author Contributions

‡These authors contributed equally to this work.

Notes

The authors declare no competing financial interest.

■ ACKNOWLEDGMENTS

This research was supported by the National Institutes of Health (RO1 EB013149) and Cancer Prevention and Research Institute of Texas (RP 120094). We also acknowledge the small animal imaging facility supported by the Cancer Center Support Grant (P30 CA 142543). We thank Dr. Nicolay Tsarevsky and Hongzhang Han for their assistance on the TGA analysis of the copolymers.

■ REFERENCES

(1) Stuart, M. A.; Huck, W. T.; Genzer, J.; Muller, M.; Ober, C.; Stamm, M.; Sukhorukov, G. B.; Szleifer, I.; Tsukruk, V. V.; Urban, M.; Winnik, F.; Zauscher, S.; Luzinov, I.; Minko, S. *Nat. Mater.* **2010**, *9*, 101.
(2) Ganta, S.; Devalapally, H.; Shahiwala, A.; Amiji, M. *J. Controlled Release* **2008**, *126*, 187.
(3) Bellomo, E. G.; Wyrsta, M. D.; Pakstis, L.; Pochan, D. J.; Deming, T. J. *Nat. Mater.* **2004**, *3*, 244.
(4) So, M. K.; Xu, C.; Loening, A. M.; Gambhir, S. S.; Rao, J. *Nat. Biotechnol.* **2006**, *24*, 339.
(5) von Maltzahn, G.; Park, J. H.; Lin, K. Y.; Singh, N.; Schwoppe, C.; Mesters, R.; Berdel, W. E.; Ruoslahti, E.; Sailor, M. J.; Bhatia, S. N. *Nat. Mater.* **2011**, *10*, 545.
(6) Whitesides, G. M.; Mathias, J. P.; Seto, C. T. *Science* **1991**, *254*, 1312.
(7) Whitesides, G. M.; Grzybowski, B. *Science* **2002**, *295*, 2418.
(8) Klouda, L.; Mikos, A. G. *Eur. J. Pharm. Biopharm.* **2008**, *68*, 34.
(9) Meyer, D. E.; Chilkoti, A. *Nat. Biotechnol.* **1999**, *17*, 1112.
(10) Li, P.; Banjade, S.; Cheng, H. C.; Kim, S.; Chen, B.; Guo, L.; Llaguno, M.; Hollingsworth, J. V.; King, D. S.; Banani, S. F.; Russo, P. S.; Jiang, Q. X.; Nixon, B. T.; Rosen, M. K. *Nature* **2012**, *483*, 336.
(11) Casey, J. R.; Grinstein, S.; Orlowski, J. *Nat. Rev. Mol. Cell Biol.* **2010**, *11*, 50.
(12) Maxfield, F. R.; McGraw, T. E. *Nat. Rev. Mol. Cell Biol.* **2004**, *5*, 121.
(13) Izumi, H.; Torigoe, T.; Ishiguchi, H.; Uramoto, H.; Yoshida, Y.; Tanabe, M.; Ise, T.; Murakami, T.; Yoshida, T.; Nomoto, M.; Kohno, K. *Cancer Treat. Rev.* **2003**, *29*, 541.
(14) Nishi, T.; Forgac, M. *Nat. Rev. Mol. Cell Biol.* **2002**, *3*, 94.
(15) Lee, J. H.; Yu, W. H.; Kumar, A.; Lee, S.; Mohan, P. S.; Peterhoff, C. M.; Wolfe, D. M.; Martinez-Vicente, M.; Massey, A. C.; Sovak, G.; Uchiyama, Y.; Westaway, D.; Cuervo, A. M.; Nixon, R. A. *Cell* **2010**, *141*, 1146.
(16) Majumdar, A.; Cruz, D.; Asamoah, N.; Buxbaum, A.; Sohar, I.; Lobel, P.; Maxfield, F. R. *Mol. Biol. Cell* **2007**, *18*, 1490.
(17) Webb, B. A.; Chimenti, M.; Jacobson, M. P.; Barber, D. L. *Nat. Rev. Cancer* **2011**, *11*, 671.
(18) Zhang, X.; Lin, Y.; Gillies, R. J. *J. Nucl. Med.* **2010**, *51*, 1167.
(19) Zhou, K.; Wang, Y.; Huang, X.; Luby-Phelps, K.; Sumer, B. D.; Gao, J. *Angew. Chem., Int. Ed. Engl.* **2011**, *50*, 6109.
(20) Zhou, K.; Liu, H.; Zhang, S.; Huang, X.; Wang, Y.; Huang, G.; Sumer, B. D.; Gao, J. *J. Am. Chem. Soc.* **2012**, *134*, 7803.
(21) Huang, X.; Huang, G.; Zhang, S.; Sagiyama, K.; Togao, O.; Ma, X.; Wang, Y.; Li, Y.; Soesbe, T. C.; Sumer, B. D.; Takahashi, M.; Sherry, A. D.; Gao, J. *Angew. Chem., Int. Ed. Engl.* **2013**, *52*, 8074.
(22) Wang, Y.; Zhou, K.; Huang, G.; Hensley, C.; Huang, X.; Ma, X.; Zhao, T.; Sumer, B. D.; DeBerardinis, R. J.; Gao, J. *Nat. Mater.* **2014**, *13*, 204.
(23) Atkins, P.; De Paula, J. *Physical Chemistry*; Oxford University Press: U.K., 2009.
(24) Yu, H.; Zou, Y.; Wang, Y.; Huang, X.; Huang, G.; Sumer, B. D.; Boothman, D. A.; Gao, J. *ACS Nano* **2011**, *5*, 9246.
(25) Tsarevsky, N. V.; Matyjaszewski, K. *Chem. Rev.* **2007**, *107*, 2270.
(26) Ma, Y.; Tang, Y.; Billingham, N. C.; Armes, S. P.; Lewis, A. L.; Lloyd, A. W.; Salvage, J. P. *Macromolecules* **2003**, *36*, 3475.
(27) Zhang, K.; Fang, H.; Wang, Z.; Li, Z.; Taylor, J. S.; Wooley, K. L. *Biomaterials* **2010**, *31*, 1805.
(28) Urano, Y.; Asanuma, D.; Hama, Y.; Koyama, Y.; Barrett, T.; Kamiya, M.; Nagano, T.; Watanabe, T.; Hasegawa, A.; Choyke, P. L.; Kobayashi, H. *Nat. Med.* **2009**, *15*, 104.
(29) Petsalakis, I. D.; Lathiotakis, N. N.; Theodorakopoulos, G. *J. Mol. Struct.: THEOCHEM* **2008**, *867*, 64.
(30) Tal, S.; Salman, H.; Abraham, Y.; Botoshansky, M.; Eichen, Y. *Chem.—Eur. J.* **2006**, *12*, 4858.
(31) Dale, T. J.; Rebek, J. *J. Am. Chem. Soc.* **2006**, *128*, 4500.
(32) Blum, G.; Mullins, S. R.; Keren, K.; Fonovic, M.; Jedeszko, C.; Rice, M. J.; Sloane, B. F.; Bogyo, M. *Nat. Chem. Biol.* **2005**, *1*, 203.
(33) Lee, S.; Ryu, J. H.; Park, K.; Lee, A.; Lee, S. Y.; Youn, I. C.; Ahn, C. H.; Yoon, S. M.; Myung, S. J.; Moon, D. H.; Chen, X.; Choi, K.; Kwon, I. C.; Kim, K. *Nano Lett.* **2009**, *9*, 4412.
(34) Levi, J.; Kothapalli, S. R.; Ma, T. J.; Hartman, K.; Khuri-Yakub, B. T.; Gambhir, S. S. *J. Am. Chem. Soc.* **2010**, *132*, 11264.
(35) Maxwell, D.; Chang, Q.; Zhang, X.; Barnett, E. M.; Piwnica-Worms, D. *Bioconjugate Chem.* **2009**, *20*, 702.
(36) Ko, J. Y.; Park, S.; Lee, H.; Koo, H.; Kim, M. S.; Choi, K.; Kwon, I. C.; Jeong, S. Y.; Kim, K.; Lee, D. S. *Small* **2010**, *6*, 2539.

Supporting Information

Ultra-pH Sensitive Nanoprobe Library with Broad pH Tunability and Fluorescence Emissions

Xinpeng Ma,[†,‡] Yiguang Wang,[†,‡]Tian Zhao,[†] Yang Li,[†] Lee-Chun Su,[†] Zhaohui Wang,[†] Gang Huang, [†]Baran D. Sumer[ξ] and Jinming Gao[*,†,&]

[†] Department of Pharmacology, [ξ]Department of Otolaryngology , Simmons Comprehensive Cancer Center, University of Texas Southwestern Medical Center, Dallas, Texas 75390, USA; [&]Department of Chemistry, University of Texas at Dallas, Richardson, Texas 75083, USA

[‡]These authors contributed equally to this work

*To whom correspondence should be addressed:

E-mail: jinming.gao@utsouthwestern.edu

Materials

The *N*-hydroxyl succinimidyl (NHS) esters of different fluorophores and fluorescence quenchers were obtained as following: RhoG-NHS, TMR-NHS, ROX-NHS, BDY-NHS, BDY-TMR-NHS, BDY630-NHS, AMCA-x-NHS, MB-NHS, PPO-NHS, QSY35, QSY7 and QSY21 ester from Invitrogen Company; Cy5-NHS, Cy5.5-NHS, Cy7.5-NHS ester from Lumiprobe Corporation; BHQ-1-NHS ester from Biosearch Technologies. PEO macroinitiator, MeO-PEO_{114}-Br, was prepared from 2-bromo-2-methyl propanoyl bromide and MeO-PEO_{114}-OH according to the procedure in the literature.[1] Bromopropane, bromobutane, bromopentane, ethanolamine and methacrylate chloride were purchased from Sigma-Aldrich. Monomers 2-(diethylamino)ethyl methacrylate (DEA-MA) and 2-aminoethyl methacrylate (AMA-MA) were purchased from Polyscience Company. AMA-MA was recrystallized twice with isopropanol and ethyl acetate (3:7). Monomer 2-(dibutylamino) ethyl methacrylate (DBA-MA) was synthesized following a previously published procedure.[2] Syntheses of 2-(dipropylamino) ethyl methacrylate (DPA-MA)and 2-(dipentylamino) ethyl methacrylate (D5A-MA) were reported recently.[3] Other solvents and reagents were used as received from Sigma-Aldrich or Fisher Scientific Inc.

Syntheses of PEO-*b*-PR block copolymers

PEO-*b*-PR copolymers were synthesized by atom transfer radical polymerization (ATRP) following similar procedures previously reported.[2] The dye free copolymers were used in polymer characterizations. PEO-*b*-PDPA is used as an example to illustrate the procedure. First, DPA-MA (1.70 g, 8 mmol), PMDETA (21 μL, 0.1 mmol) and MeO-PEO_{114}-Br (0.5 g, 0.1 mmol) were charged into a polymerization tube. Then a mixture of 2-propanol (2 mL) and DMF (2 mL) was added to dissolve the monomer and initiator. After three cycles of freeze-pump-thaw to remove the oxygen, CuBr (14 mg, 0.1 mmol) was added into the polymerization tube under nitrogen atmosphere, and the tube was sealed *in vacuo*. The polymerization was carried out at 40 °C for 8 hours. After polymerization, the reaction mixture was diluted with 10 mL THF, and passed through a neutral Al_2O_3 column to remove the catalyst. The THF solvent was removed by rotovap. The residue was dialyzed in distilled water and lyophilized to obtain a white powder. After syntheses, the polymers were characterized by ^{1}H NMR, ^{13}C NMR, gel permeation chromatography (GPC), differential scanning calorimetry (DSC) and thermal gravimetric analysis (TGA). All the NMR spectra were obtained in $CDCl_3$ using tetramethylsilane (TMS) as the internal reference on a Varian 400 MHz ^{1}H NMR spectrometer. GPC measurements were performed on a Viscotech GPCmax instrument using PLgel 5μm MIXED-D columns (Polymer Labs) and THF as eluent (1 mL/min). DSC analysis of copolymers was carried out using a Shimadzu Differential Scanning Calorimeter (DSC-60, Columbia, USA) with samples under a nitrogen atmosphere to determine the glass transition temperature (T_g) and melting temperature (T_m). DSC measurements were performed at a heating rate of 10˚C/min in the temperature range of -100˚C to 100 ˚C and sequential cooling back to -100 ˚C at a cooling rate of 50 ˚C/min, and then the sample was heated at a rate of 10 ˚C/min again. The data were analyzed using the TA software. T_g was calculated as the midpoint temperature during glass transition. TGA

experiments were conducted using a Perkin-Elmer TGA-4000 instrument (Waltham, MA) under a nitrogen atmosphere (flow rate: 20 mL/min). TGA measurements were performed at a heating rate of 20 ˚C/min in the temperature range of 30 ˚C to 500 ˚C. The onset degradation temperature (T_d, ˚C) and temperature with 50% weight loss (T_{50}) were determined by the Paris Data Analysis software.

The ^{1}H and ^{13}C NMR, DSC and TGA characterizations of all the copolymers are as following:

PEO-*b*-PD5A

^{1}H NMR (TMS, $CDCl_3$, ppm): 3.97 (b, 160H, $COOCH_2$), 3.79-3.50 (m, 450H, OCH_2CH_2O), 3.38 (s, 3H, CH_3O), 2.67 (b, 160H, $COOCH_2CH_2N$), 2.45 (b, 320H, NCH_2CH_2), 1.88-1.73 (m, 166H, CCH_3C& $C(CH_3)_2$), 1.43 (m, 320H, NCH_2CH_2), 1.32 (m, 320H, $NCH_2CH_2CH_2$), 1.27 (m, 320H, CH_2CH_3), 1.04 (b, 160H, CCH_3), 0.91 (m, 480H, CH_2CH_3). **^{13}C NMR** ($CDCl_3$, ppm):177.55, 177.16, 176.40, 71.88, 70.51, 63.08, 59.00, 58.51, 54.77, 54.66, 51.64, 45.9, 44.66, 29.62, 27.06, 22.64, 18.61, 18.30, 16.71, 14.14. See Table S3 for DSC and TGA data.

PEO-*b*-P(DEA_{20}-*r*-$D5A_{60}$)

^{1}H NMR (TMS, $CDCl_3$, ppm):): 3.98 (b, 160H, $COOCH_2$), 3.79-3.50 (m, 450H, OCH_2CH_2O), 3.38 (s, 3H, CH_3O), 2.67 (b, 160H, $COOCH_2CH_2N$), 2.57 (b, 40H, $COOCH_2CH_2NEt_2$), 2.44(b, 240H, NCH_2CH_2), 1.89-1.79 (m, 166H, CCH_2C& $C(CH_3)_2$), 1.43 (m, 240H, NCH_2CH_2), 1.32 (m, 240H, NCH_2CH_2 CH_2), 1.26 (b, 240H, $CH_2CH_2CH_3$), 1.04 (b, 240H, NCH_2CH_3), 0.91 (m, 520H, CCH_3 & $CH_2CH_2CH_3$).). **^{13}C NMR** ($CDCl_3$, ppm): 177.60, 177.21, 176.40, 71.86, 70.51, 63.11, 54.78, 54.66, 52.06, 51.63, 50.43, 47.58, 45.05, 44.67, 29.61, 27.07, 22.64, 18.60, 18.29, 16.92, 16.58, 14.14, 12.15. T_g: 0.55 ˚C. T_m: 49.3 ˚C. T_d: 258.8 ˚C. T_{50}: 394.8 ˚C.

PEO-*b*-P(DEA_{40}-*r*-$D5A_{40}$)

^{1}H NMR (TMS, $CDCl_3$, ppm):): 3.98 (b, 160H, $COOCH_2$), 3.81-3.50 (m, 450H, OCH_2CH_2O), 3.40 (s, 3H, CH_3O), 2.69 (b, 160H, $COOCH_2CH_2N$), 2.57 (b, 160H, $COOCH_2CH_2NEt_2$), 2.44(b, 160H, NCH_2CH_2), 1.89-1.79 (m, 166H, CCH_2C& $C(CH_3)_2$), 1.43 (m, 160H, NCH_2CH_2), 1.32 (m, 160H, NCH_2CH_2 CH_2), 1.25 (b, 160H, $CH_2CH_2CH_3$), 1.05 (b, 240H, NCH_2CH_3), 0.91 (m, 400H, CCH_3 & $CH_2CH_2CH_3$).). **^{13}C NMR** ($CDCl_3$, ppm): 177.62, 177.25, 176.46, 71.84, 70.50, 63.09, 56.70, 54.66, 54.14, 51.62, 50.41, 47.57, 45.02, 44.65, 29.61, 27.05, 22.63, 20.58, 18.48, 16.86, 16.60, 14.13, 12.12, 11.85. T_g: 1.2 ˚C. T_m: 45.1 ˚C. T_d: 265.2 ˚C. T_{50}: 400.1 ˚C.

PEO-*b*-P(DEA_{60}-*r*-$D5A_{20}$)

^{1}H NMR (TMS, $CDCl_3$, ppm):): 3.93 (b, 160H, $COOCH_2$), 3.72-3.44 (m, 450H, OCH_2CH_2O), 3.32 (s, 3H, CH_3O), 2.64 (b, 160H, $COOCH_2CH_2N$), 2.51 (b, 240H, $COOCH_2CH_2NEt_2$), 2.39 (b, 80H, NCH_2CH_2), 1.82-1.73 (m, 166H, CCH_2C& $C(CH_3)_2$), 1.38 (m, 80H, NCH_2CH_2), 1.27 (m, 80H, NCH_2CH_2 CH_2), 1.20 (b, 80H, $CH_2CH_2CH_3$), 0.99 (b, 360H, NCH_2CH_3), 0.85 (m, 280H,

C*C*H_3 & $CH_2CH_2CH_2CH_3$).). **^{13}C NMR** ($CDCl_3$, ppm): 177.67, 177.31, 176.46, 71.87, 70.45, 63.17, 58.99, 54.63, 54.13, 51.57, 50.38, 47.53, 45.02, 44.64, 29.59, 26.95, 22.60, 18.53, 16.82, 16.61, 14.11, 12.01. T_g: 1.9 ˚C. T_m: 45.7 ˚C. T_d: 276.3 ˚C. T_{50}: 407.7 ˚C.

PEO-*b*-PDEA

^{1}H NMR (TMS, $CDCl_3$, ppm): 3.93 (b, 160H, COOCH_2), 3.73-3.42 (m, 450H, OCH_2CH_2O), 3.31 (s, 3H, CH_3O), 2.64 (b, 166H, $COOCH_2CH_2N$), 2.51 (b, 320H, NCH_2CH_3), 1.82-1.73 (m, 160H, CCH_2C& $C(CH_3)_2$), 1.18 (s, 6H, $C(CH_3)_2$), 0.99 (m, NCH_2CH_3), 0.82 (b, 160H, CCH_3).). **^{13}C NMR** ($CDCl_3$, ppm): 177.61, 177.22, 176.44, 71.79, 70.42, 63.13, 58.89, 54.58, 54.10, 50.36, 50.30, 47.50, 44.93, 44.55, 29.52, 18.39, 16.73, 12.04. T_g: 2.3 ˚C. T_m: 56.4 ˚C. T_d: 287.8 ˚C. T_{50}: 418.8 ˚C.

PEO-*b*-PDBA

^{1}H NMR (TMS, $CDCl_3$, ppm): 3.91 (b, 160H, COOCH_2), 3.73-3.42 (m, 450H, OCH_2CH_2O), 3.31 (s, 3H, CH_3O), 2.60 (b, 166H, $COOCH_2CH_2N$), 2.38 (b, 320H, NCH_2CH_2), 1.82-1.72 (m, 160H, CCH_3C& $C(CH_3)_2$), 1.35 (m, 320H, NCH_2CH_2), 1.25 (m, 320H, $CH2CH_2CH_3$), 0.97-0.84 (m, 640H, CH_2CH_3& CCH_3). **^{13}C NMR** ($CDCl_3$, ppm): 177.58, 177.19, 176.48, 71.90, 70.50, 63.08, 58.97, 57.47, 54.38, 52.03, 51.65, 45.05, 44.63, 29.55, 29.47, 20.51, 18.27, 16.79, 16.61, 14.08, 14.01. See Table S3 for DSC and TGA data.

PEO-*b*-P(DPA$_{20}$-*r*-DBA$_{60}$)

^{1}H NMR (TMS, $CDCl_3$, ppm): 3.97 (b, 160H, COOCH_2), 3.83-3.45 (m, 450H, OCH_2CH_2O), 3.38 (s, 3H, CH_3O), 2.67 (b, 166H, $COOCH_2CH_2N$), 2.44 (b, 320H, NCH_2CH_2), 1.80-1.68 (m, 160H, CCH_3C& $C(CH_3)_2$), 1.42 (m, 320H, NCH_2CH_2), 1.30 (m, 240H, $NCH_2CH_2CH_2CH_3$), 1.04-0.87 (m, 640H, CH_2CH_3& CCH_3).). **^{13}C NMR** ($CDCl_3$, ppm): 177.63, 177.23, 176.47, 71.87, 70.51, 63.19, 63.13, 63.01, 56.71, 54.40, 51.67, 45.06, 44.65, 29.57, 20.58, 20.53, 18.51, 17.00, 16.64, 14.09, 11.84. T_g: 5.8 ˚C. T_m: 51.1 ˚C. T_d: 242.3 ˚C. T_{50}: 383.7 ˚C.

PEO-*b*-P(DPA$_{40}$-*r*-DBA$_{40}$)

^{1}H NMR (TMS, $CDCl_3$, ppm): 3.98 (b, 160H, COOCH_2), 3.83-3.45 (m, 450H, OCH_2CH_2O), 3.38 (s, 3H, CH_3O), 2.67 (b, 160H, $COOCH_2CH_2N$), 2.43 (b, 320H, NCH_2CH_2), 1.91-1.80 (m, 166H, CCH_3C& $C(CH_3)_2$), 1.44 (m, 320H, NCH_2CH_2), 1.32 (m, 160H, $NCH_2CH_2CH_2CH_3$), 1.04-0.87 (m, 640H, CH_2CH_3& CCH_3).). **^{13}C NMR** ($CDCl_3$, ppm): 177.64, 177.26, 176.44, 70.46, 63.21, 63.07, 56.69, 54.48, 54.39, 51.71, 45.05, 44.64, 29.50, 20.53, 18.48, 18.33, 16.80, 16.46, 14.08, 11.83. T_g: 4.2 ˚C. T_m: 49.6 ˚C. T_d: 260.5 ˚C. T_{50}: 390.8 ˚C.

PEO-*b*-P(DPA$_{60}$-*r*-DBA$_{20}$)

^{1}H NMR (TMS, $CDCl_3$, ppm): 3.97 (b, 160H, COOCH_2), 3.82-3.47 (m, 450H, OCH_2CH_2O), 3.38 (s, 3H, CH_3O), 2.67 (b, 160H, $COOCH_2CH_2N$), 2.41 (b, 320H, NCH_2CH_2), 1.90-1.80 (m, 166H, CCH_3C& $C(CH_3)_2$), 1.44 (m, 320H, NCH_2CH_2), 1.30 (m, 80H, $CH2CH_2CH_3$), 1.04-0.87

(m, 640H, CH_2CH_3& CCH_3). **^{13}C NMR** ($CDCl_3$, ppm): 177.67, 177.29, 176.54, 71.84, 70.46, 63.20, 63.06, 56.69, 54.47, 54.39, 51.70, 45.04, 44.64, 29.63, 29.48, 20.51, 18.48, 16.81, 16.57, 14.08, 11.83. See Table S3 for DSC and TGA data.

PEO-*b*-PDPA

^{1}H NMR (TMS, $CDCl_3$, ppm): 3.97 (b, 160H, $COOCH_2$), 3.83-3.47 (m, 450H, OCH_2CH_2O), 3.38 (s, 3H, CH_3O), 2.67 (b, 160H, $COOCH_2CH_2N$), 2.41 (b, 320H, NCH_2CH_2), 1.90-1.80 (m, 166H, CCH_3C& $C(CH_3)_2$), 1.44 (m, 320H, $NCH_2CH_2CH_3$), 1.04-0.87 (m, 640H, CH_2CH_3& CCH_3). **^{13}C NMR** ($CDCl_3$, ppm): 177.65, 177.27, 176.52, 71.85, 70.49, 63.20, 63.05, 58.96, 56.69, 54.14, 51.70, 45.02, 44.62, 29.61, 20.73, 20.56, 18.42, 16.55, 11.81. See Table S3 for DSC and TGA data.

PEO-*b*-P(DBA$_{28}$-*r*-D5A$_{52}$)

^{1}H NMR (TMS, $CDCl_3$, ppm): 3.97 (b, 160H, $COOCH_2$), 3.83-3.45 (m, 450H, OCH_2CH_2O), 3.38 (s, 3H, CH_3O), 2.67 (b, 160H, $COOCH_2CH_2N$), 2.44 (b, 320H, NCH_2CH_2), 1.89-1.80 (m, 166H, CCH_3C & $C(CH_3)_2$), 1.42 (m, 320H, NCH_2CH_2), 1.32 (m, 528H, $NCH_2CH_2CH_2CH_3$ & $NCH_2CH_2CH_2$ CH_2CH_3), 1.04-0.91 (m, 640H, CCH_3 & CH_2CH_3). **^{13}C NMR** ($CDCl_3$, ppm): 177.59, 177.18, 176.46, 71.89. 70.52, 63.63, 63.10, 54.67, 54.40, 51.65, 45.09, 44.67, 30.58, 29.62, 28.50, 27.07, 25.44, 25.12, 24.68, 22.65, 22.17, 20.55, 19.72, 18.58, 18.31, 18.19, 16.63, 15.47, 14.14. See Table S3 for DSC and TGA data.

PEO-*b*-P(DBA$_{56}$-*r*-D5A$_{24}$)

^{1}H NMR (TMS, $CDCl_3$, ppm): 3.97 (b, 160H, $COOCH_2$), 3.83-3.45 (m, 450H, OCH_2CH_2O), 3.38 (s, 3H, CH_3O), 2.67 (b, 160H, $COOCH_2CH_2N$), 2.46 (b, 320H, NCH_2CH_2), 1.89-1.79 (m, 166H, CCH_3C & $C(CH_3)_2$), 1.42 (m, 320H, NCH_2CH_2), 1.34 (m, 416H, $NCH_2CH_2CH_2CH_3$ & $NCH_2CH_2CH_2$ CH_2CH_3), 1.04-0.87 (m, 640H, CCH_3 & CH_2CH_3). **^{13}C NMR** ($CDCl_3$, ppm): 177.58, 177.18, 176.44, 71.87, 70.50, 63.12, 54.66, 54.39, 51.67, 45.07, 44.64, 29.58, 28.32, 27.05, 25.73, 25.42, 25.10, 22.62, 21.67, 20.52, 19.40, 18.56, 17.70, 16.59, 16.06, 14.09. See Table S3 for DSC and TGA data.

PEO-*b*-P(DPA$_{30}$-*r*-DBA$_{50}$)

^{1}H NMR (TMS, $CDCl_3$, ppm): 3.97 (b, 160H, $COOCH_2$), 3.83-3.45 (m, 450H, OCH_2CH_2O), 3.38 (s, 3H, CH_3O), 2.67 (b, 166H, $COOCH_2CH_2N$), 2.43 (b, 320H, NCH_2CH_2), 1.89-1.68 (m, 160H, CCH_3C & $C(CH_3)_2$), 1.42 (m, 320H, NCH_2CH_2), 1.32 (m, 200H, $NCH_2CH_2CH_2CH_3$), 1.04-0.87 (m, 640H, CH_2CH_3& CCH_3). **^{13}C NMR** ($CDCl_3$, ppm):177.64, 177.24, 176.52, 71.89, 70.52, 63.13, 59.00, 56.72, 54.42, 51.74, 51.68, 45.07, 44.66, 29.66, 29.58, 22.64, 20.59, 20.54, 18.51, 16.93, 16.63, 14.11, 11.85. See Table S3 for DSC and TGA data.

PEO-*b*-P(DEA$_{21}$-*r*-DPA$_{79}$)

^{1}H NMR (TMS, $CDCl_3$, ppm): 3.98 (b, 200H, COOCH_2), 3.83-3.47 (m, 450H, OCH_2CH_2O), 3.38 (s, 3H, CH_3O), 2.68 (b, 200H, COOCH$_2$CH_2N), 2.57 (b, 84H, NCH_2CH$_3$), 2.41 (b, 316H, NCH_2CH$_2$), 1.90-1.80 (m, 206H, CCH_3C & C(CH_3)$_2$), 1.46 (m, 316H, NCH$_2$CH_2CH$_3$), 1.05-0.89 (m, 900H, CH$_2$CH_3& CCH_3). **^{13}C NMR** ($CDCl_3$, ppm): 177.67, 177.28, 176.54, 71.86, 70.49, 63.21, 63.06, 56.69, 54.64, 54.18, 51.71, 50.38, 47.57, 45.02, 44.63, 29.62, 20.56, 18.42, 16.81, 16.55, 12.10, 11.82. See Table S3 for DSC and TGA data.

PEO-*b*-P(DEA$_{39}$-*r*-DPA$_{61}$)

^{1}H NMR (TMS, $CDCl_3$, ppm): 3.99 (b, 200H, COOCH_2), 3.83-3.45 (m, 450H, OCH_2CH_2O), 3.38 (s, 3H, CH_3O), 2.69 (b, 200H, COOCH$_2$CH_2N), 2.57 (b, 156H, NCH_2CH$_3$), 2.41 (b, 244H, NCH_2CH$_2$), 1.89-1.80 (m, 206H, CCH_3C & C(CH_3)$_2$), 1.45 (m, 244H, NCH$_2$CH_2CH$_3$), 1.05-0.87 (m, 900H, CH$_2$CH_3& CCH_3). **^{13}C NMR** ($CDCl_3$, ppm):177.63, 177.26, 176.51, 71.83, 70.47, 63.19, 63.04, 58.94, 56.66, 54.59, 54.22, 51.68, 50.40, 47.54, 44.98, 44.60, 29.58, 20.53, 18.41, 16.79, 16.49, 12.08, 11.80. See Table S3 for DSC and TGA data.

PEO-*b*-P(DEA$_{58}$-*r*-DPA$_{42}$)

^{1}H NMR (TMS, $CDCl_3$, ppm): 3.99 (b, 200H, COOCH_2), 3.83-3.45 (m, 450H, OCH_2CH_2O), 3.38 (s, 3H, CH_3O), 2.69 (b, 200H, COOCH$_2$CH_2N), 2.57 (b, 232H, NCH_2CH$_3$), 2.41 (b, 168H, NCH_2CH$_2$), 1.89-1.80 (m, 206H, CCH_3C & C(CH_3)$_2$), 1.46 (m, 168H, NCH$_2$CH_2CH$_3$), 1.04 (m, 474H, CH$_2$CH_3& CCH_3), 0.89 (m, 426H, CH$_2$CH_3& CCH_3). **^{13}C NMR** ($CDCl_3$, ppm): 177.66, 177.29, 176.52, 71.85, 70.48, 63.20, 63.05, 56.68, 54.17, 51.70, 50.41, 50.36, 47.56, 45.01, 44.62, 29.61, 20.55, 18.40, 16.71, 16.57, 12.10, 11.82. See Table S3 for DSC and TGA data.

Synthesis of triblock copolymer (PEG-*b*-P(R$_1$-*b*-R$_2$)) for control studies

PEG-*b*-P(R$_1$-*b*-R$_2$) triblock copolymers were synthesized by ATRP method following similar procedures previously reported.[2] PEO-*b*-P(D5A-*b*-DEA) is used as an example to illustrate the procedure. First, D5A-MA (0.54 g, 2 mmol), PMDETA (12μL, 0.05 mmol) and MeO-PEO$_{114}$-Br (0.25 g, 0.05 mmol) were charged into a polymerization tube. Then a mixture of 2-propanol (1 mL) and DMF (1 mL) was added to dissolve the monomer and initiator. After three cycles of freeze-pump-thaw to remove the oxygen, CuBr (7 mg, 0.05 mmol) was added into the polymerization tube under nitrogen atmosphere, and the tube was sealed *in vacuo*. After polymerization carrying out at 40 °C for 8 hours, deoxygenized DEA-MA (0.368, 2 mmol) was injected to the reaction solution via air-tight syringe and the reaction mixture was stirred at 40 °C for additional 8 hours. After polymerization, the reaction mixture was diluted with 10 mL THF, and passed through a neutral Al_2O_3 column to remove the catalyst. The THF solvent was removed by rotovap. The residue was dialyzed in distilled water and lyophilized to obtain a white powder. The ^{1}H NMR, ^{13}C NMR and GPC characterizations of the two copolymers are as following:

PEG-*b*-P(D5A-*b*-DEA)

^{1}H NMR (TMS, $CDCl_3$, ppm): 3.91 (b, 160H, $COOCH_2$), 3.75-3.40 (m, 450H, OCH_2CH_2O), 3.31 (s, 3H, CH_3O), 2.61 (b, 160H, $COOCH_2CH_2N$), 2.50 (b, 160H, $COOCH_2CH_2NEt_2$), 2.38(b, 160H, NCH_2CH_2), 1.82-1.74 (m, 166H, CCH_2C & $C(CH_3)_2$), 1.35 (b, 80H, NCH_2CH_2), 1.25 (m, 160H, $NCH_2CH_2CH_2$), 0.97 (b, 120H, NCH_2CH_3), 0.85 (m, 280H, CCH_3 & $CH_2CH_2CH_3$).). **^{13}C NMR** ($CDCl_3$, ppm): 177.52, 177.19, 176.35, 74.74, 71.80, 70.44, 63.09, 58.89, 56.64, 54.33, 51.46, 44.95, 44.55, 29.51, 20.51, 20.45, 18.43, 16.50, 14.07, 11.76. *Mn*: 22.1 kDa. PDI: 1.34.

PEG-*b*-P(DBA-*b*-DPA)

^{1}H NMR (TMS, $CDCl_3$, ppm): 3.91 (b, 160H, $COOCH_2$), 3.75-3.40 (m, 450H, OCH_2CH_2O), 3.31 (s, 3H, CH_3O), 2.61 (b, 160H, $COOCH_2CH_2N$), 2.38 (b, 320H, NCH_2CH_2), 1.87-1.74 (m, 166H, CCH_3C & $C(CH_3)_2$), 1.36 (m, 320H, NCH_2CH_2), 1.25 (m, 160H, $NCH_2CH_2CH_2CH_3$), 0.98-0.85 (m, 640H, CH_2CH_3& CCH_3).). **^{13}C NMR** ($CDCl_3$, ppm): 177.52, 177.19, 176.35, 71.80, 70.44, 63.09, 58.89, 56.64, 54.33, 51.64, 44.95, 44.55, 30.31, 29.51, 20.51, 20.45, 18.43, 16.78, 16.50, 14.02, 11.76. *Mn*: 20.9 kDa. PDI: 1.42.

Syntheses of PEO-*b*-(PR-*r*-Dye/FQ) block copolymers

AMA-MA was used for the conjugation of dyes or fluorescence quenchers. Synthesis of PEO-*b*-(PR-*r*-AMA) copolymers followed the procedure described above. Three primary amino groups were introduced into each polymer chain by controlling the feeding ratio of AMA monomer to the initiator (ratio = 3). After synthesis, PEO-*b*-(PR-*r*-AMA) (10 mg) was dissolved in 2 mL DMF. Then the NHS-ester (1.5 equivalences for Dye-NHS or FQ-NHS) was added. After overnight reaction, the copolymers were purified by preparative gel permeation chromatography (PLgel Prep 10 m 10E3 Å 300×250 columns by Varian, THF as eluent at 5 mL/min) to remove the free dye molecules. The produced PEO-*b*-(PR-*r*-Dye/FQ) copolymers were lyophilized and kept at -20 °C for storage.

Preparation and Characterization of micelle nanoparticles

Micelles were prepared following a previously published procedure.[2] In a typical procedure, 5 mg of **PDPA-Cy5** was dissolved in 0.5 mL THF. Then, the solution was slowly added into 4 mL of Milli-Q deionized water under sonication. The mixture was filtered 4 times to remove THF using the micro-ultrafiltration system (MWCO = 100 KD). Then, the deionized water was added to adjust the polymer concentration to 5 mg/mL as a stock solution. For the mixed micelles, different weight ratios of the PR-Dye and PR-FQ copolymers were dissolved in 0.5 mL THF, and the same procedure was used. After micelle formation, the nanoparticles were characterized by transmission electron microscopy (TEM, JEOL 1200 EX model, Tokyo, Japan) to examine micelle size and morphology, dynamic light scattering (DLS, Malvern Nano-ZS model, He-Ne laser, λ= 633 nm) for hydrodynamic diameter (D_h). The zeta-potential was measured using a folded capillary cell (Malvern Instruments, Herrenberg, Germany). The presented data were averaged from three independent measurements.

Fluorescence characterization

The fluorescence emission spectra were obtained on a Hitachi fluorometer (F-7500 model, Tokyo, Japan). For each copolymer, the sample was initially prepared in Milli-Q water at the concentration of 2 mg/mL. Then the stock solution was diluted in 0.2 M citric-phosphate buffers (containing 0.15 M sodium chloride) at different pH values. The terminal polymer concentration was controlled at 100-200 μg/mL.

The fluorescent images of **4.4-7.1-Cy5s**, **5.0-BDY**, **5.3-RhoG**, **5.6-TMR**, **5.9-ROX**, **6.2-BDY630**, **6.5-Cy5**, **6.8-Cy5.5** and **7.1-Cy7.5** solutions at different pH values (100 μg/mL for each sample) were obtained using the Maestro imaging system (CRI, Inc., Woburn, MA) with a proper band pass excitation filter and long-pass emission filter according to the instrument manual. For **4.4-AMCA** and **4.7-MB** solutions, the images were taken by a camera under the irradiation of a handheld UV light (365 nm). All measurements were conducted at room temperature.

Measurement of dye conjugation efficiency

The dye conjugation number and efficiency were determined by a UV-Vis method. Typically, solutions of the dye reference standard and polymer test samples in methanol were prepared. Then, the absorbance of the standard and sample solutions was determined at corresponding peak wavelength. The dye conjugation number and efficiency were calculated using the following equations:

$$N_{dye} = \frac{C_{dye}}{A_{dye}} \frac{A_{polymer}}{C_{polymer}} \frac{MW_{polymer}}{MW_{dye}}$$

$$Efficiency\ (\%) = \frac{N_{dye}}{N_{NH2}} \times 100\%$$

Where N_{dye} and N_{NH2} are the conjugated dye number and number of primary amine in the polymer; A_{dye} and $A_{polymer}$ are the absorbance of dye reference standard and polymer test sample, respectively; C_{dye} and $C_{polymer}$ are the concentrations of dye reference standard and polymer test sample, respectively; MW_{dye} and $MW_{polymer}$ are the molecular weights of dye reference standard and polymer test sample, respectively.

Quantum yields of fluorescent nanoprobes

The relative fluorescent quantum yield is measured via the comparative method described in the literature[4]. To simplify the test, the well characterized standards of known Φ_F were used as reference for the determination of quantum yield of dye-conjugated polymers. The reference dyes chosen for conjugation include Marina blue, BDY493, TMR, and Cy5, which have reported quantum yields of 0.89, 0.90, 0.68, and 0.28 in methanol, respectively[5-7].

For the quantum yield measurement, the free dyes and dye-conjugated polymers were dissolved and diluted in methanol to keep the absorbance of the solution less than 0.05. Then, the fluorescence spectra of the prepared samples were measured using an excitation wavelength

same as the absorbance wavelength. The integrated fluorescence intensities of the two solutions were calculated from the spectra. The quantum yield of the dye-conjugated polymers was calculated using the following equation:

$$\Phi_F = \Phi_{F,R} \frac{I}{OD} \frac{OD_R}{I_R} \frac{n^2}{n_R^2}$$

Where Φ_F is the fluorescent quantum yield, *I* is the integrated emission intensities, *OD* is the absorbance, *n* is the refractive index of the solvent, and the subscript *R* denotes the values for the reference sample.

Nanoprobe stability in serum and solutions containing serum components

Fresh mouse serum was collected and filtered through 0.22 μm syringe filters. Mouse serum components, including albumin and γ-globulin were obtained from Sigma-Aldrich Inc. Typically, 40 μL of nanoprobe (5 mg/mL) was added to 1 ml of serum or serum components. The mixture was incubated at 37ºC in a humidified chamber. At each designated time point, 100 μL aliquots of mixture were collected and immediately determined at pH 7.4 and pH 5.0 on a Hitachi fluorometer (F-7500 model, Tokyo, Japan) to calculate the fluorescence activation ratios.

Cytotoxicity analysis of polymer nanoprobes

H2009 lung cancer cells were plated onto 96-well plates at a density of 10,000 cells/well and incubated in the RPMI 1640 medium containing 5% fetal bovine serum (FBS) at 37 ℃ , 5% CO_2/95% air to allow cell growth for 24 hours. Then the cells were exposed to increasing concentrations of a series of polymer nanoprobes for 4 hours and washed three times with PBS, and the fresh medium was added into plates. The cells were incubated for 48 hours before determination of cell viability. The cell viability was measured using an MTT assay. Briefly, after drug exposure, the cells were incubated with 0.5 mg/mL MTT solution for 4 hours, after which the medium was removed. Two hundred μL of DMSO was added into cell plates for OD determination at 570 nm using a microplate reader (SpectraMax M5, Molecular Devices, CA) to determine the dose-response relationships.

Confocal imaging of nanoprobe uptake in H2009 cells

H2009 lung cancer cells were plated in glass bottom dishes (MatTek, MA) in 1 mL phenol red-free RPMI medium and incubated with nanoprobes, including probe 6.2-BDY493 W/WO BHQ1 as well as probe 6.2-MB W/WO QSY35, at a polymer concentration of 200 μg/mL at pH 7.4. Confocal images were captured 60 min after addition of nanoprobes using the Nikon ECLIPSE TE2000-E confocal microscope with a 100× objective lens. MB and BDY493 were excited at 405 and 488 nm, respectively. The emission wavelengths of MB and BDY493 were 460 and 515 nm, respectively. The images were analyzed using Image-J software. Five independent measurements were presented as the mean ± standard deviation.

Reference

1. Bronstein, L. M.; Sidorov, S. N.; Zhirov, V.; Zhirov, D.; Kabachii, Y. A.; Kochev, S. Y.; Valetsky, P. M.; Stein, B.; Kiseleva, O. I.; Polyakov, S. N.; Shtykova, E. V.; Nikulina, E. V.; Svergun, D. I.; Khokhlov, A. R., *J. Phys. Chem. B* **2005,***109* (40), 18786-98.
2. Zhou, K.; Wang, Y.; Huang, X.; Luby-Phelps, K.; Sumer, B. D.; Gao, J., Tunable, Ultra-Sensitive pH Responsive Nanoparticles Targeting Specific Endocytic Organelles in Living Cells.*Angew. Chem. Int. Ed. Engl.* **2011,***50* (27), 6109-14.
3. Yang L, Wang YG, Huang G, Ma X, Gao J. A Surprising Chaotropic Anion-Induced Supramolecular Self-Assembly of Ionic Polymeric Micelles. *Angew. Chem. Int. Ed.* DOI: 10.1002/anie.201402525.
4. Lakowicz J.R., Principles of Fluorescence Spectroscopy, 2nd Ed., Kluwer Academic, New York, 1999.
5. Toomre, D. & Manstein, D.J. Lighting up the cell surface with evanescent wave microscopy. *Trends in cell biology* 2001, 11, 298-303.
6. Haugland, R.P. A guide to fluorescent probes and labeling technologies. 10th Edition. Invitrogen, San Diego, 2005.
7. Sun, W.C., Gee, K.R. & Haugland, R.P. Synthesis of novel fluorinated coumarins: excellent UV-light excitable fluorescent dyes. Bioorganic & medicinal chemistry letters 1998, 8, 3107-3110.

Table S1. Coarse-tuned pH sensitive nanoprobes from Cy5-conjugated **PEO-P(DEA$_x$-D5A$_y$)** copolymers.

Polymers	M_n (kDa)	M_w (kDa)	PDI	Yield (%)	pK_a	pH_t	$\Delta pH_{10\text{-}90\%}$
PD5A	26.9	32.6	1.21	85	4.25	4.38	0.19
P(DEA$_{20}$-D5A$_{60}$)	21.3	26.3	1.23	90	5.20	5.19	0.65
P(DEA$_{40}$-D5A$_{40}$)	21.3	25.8	1.20	95	6.07	5.99	0.64
P(DEA$_{60}$-D5A$_{20}$)	22.3	26.4	1.19	90	6.70	6.88	0.47
PDEA	22.6	26.6	1.18	91	7.43	7.83	0.14

Table S2. Fine-tuned pH sensitive nanoprobes from Cy5-conjugated **PEO-P(DPA$_x$-DBA$_y$)** copolymers.

Polymers	M_n (kDa)	M_w (kDa)	PDI	Yield (%)	pK_a	pH_t	$\Delta pH_{10\text{-}90\%}$
PDBA	22.5	26.8	1.19	80	5.17	5.27	0.20
P(DPA$_{20}$-DBA$_{60}$)	19.7	21.4	1.09	94	5.40	5.46	0.19
P(DPA$_{40}$-DBA$_{40}$)	21.7	24.7	1.14	78	5.63	5.70	0.20
P(DPA$_{60}$-DBA$_{20}$)	23.9	27.9	1.17	83	5.81	5.91	0.18
PDPA	22.6	27.3	1.21	91	6.18	6.21	0.20

Table S3. Characterization of the copolymers from the UPS library spanning the pH range from 4.4 to 7.4.

Probe	Composition	M_n (kDa)	M_w (kDa)	PDI	Yield (%)	T_g (°C)	T_m (°C)	T_d (°C)	T_{50} (°C)
4.4	PD5A	26.9	32.6	1.21	85	3.2	42.0	247.1	379.6
4.7	P(DBA$_{28}$-D5A$_{52}$)	20.2	23.3	1.15	82	3.0	42.3	249.8	395.4
5.0	P(DBA$_{56}$-D5A$_{24}$)	20.0	25.9	1.29	84	-[a]	44.4	257.7	396.8
5.3	PDBA	22.5	26.8	1.19	80	2.5	44.9	259.1	425.5
5.6	P(DPA$_{30}$-DBA$_{50}$)	20.4	24.9	1.22	89	3.7	48.1	253.3	400.6
5.9	P(DPA$_{60}$-DBA$_{20}$)	23.9	27.9	1.17	83	-1.9	47.9	258.8	386.2
6.2	PDPA	20.1	23.3	1.21	91	4.0	58.7	244.6	403.3
6.5	P(DEA$_{21}$-DPA$_{79}$)	21.8	24.3	1.12	87	0.16	45.4	267.2	402.3
6.8	P(DEA$_{39}$-DPA$_{61}$)	20.3	23.2	1.14	82	1.2	47.4	278.2	411.2
7.1	P(DEA$_{58}$-DPA$_{42}$)	23.1	25.2	1.09	85	0.20	47.1	280.3	406.7
7.4	P(DEA$_{76}$-DPA$_{24}$)	22.5	25.4	1.13	87	1.2	48.1	283.0	414.4

[a] Not detectable

Table S4. Characterization of the Cy5-conjugated nanoprobes from the UPS library.

Probe	Composition	D_h (nm)	PDI	Zeta-potential (mV)	pK_a	pH_t	$\Delta pH_{10\text{-}90\%}$
4.4	PD5A	50.8 ± 3.0	0.13	-0.6 ± 1.2	4.25	4.38	0.19
4.7	$P(DBA_{28}\text{-}D5A_{52})$	68.9 ± 2.6	0.09	-0.3 ± 0.6	4.58	4.67	0.15
5.0	$P(DBA_{56}\text{-}D5A_{24})$	63.2 ± 3.2	0.09	-2.0 ± 1.0	4.93	4.96	0.18
5.3	PDBA	43.5 ± 6.6	0.13	-1.3 ± 1.1	5.17	5.27	0.20
5.6	$P(DPA_{30}\text{-}DBA_{50})$	55.7 ± 1.4	0.12	-1.1 ± 0.7	5.60	5.63	0.19
5.9	$P(DPA_{60}\text{-}DBA_{20})$	49.3 ± 2.7	0.11	-0.2 ± 0.6	5.81	5.91	0.18
6.2	PDPA	46.8 ± 2.0	0.12	-0.3 ± 0.7	6.18	6.21	0.20
6.5	$P(DEA_{21}\text{-}DPA_{79})$	45.6 ± 3.3	0.12	0.4 ± 1.4	6.46	6.45	0.19
6.8	$P(DEA_{39}\text{-}DPA_{61})$	36.2 ± 1.6	0.13	-2.0 ± 0.7	6.76	6.76	0.20
7.1	$P(DEA_{58}\text{-}DPA_{42})$	35.6 ± 2.4	0.17	-1.1 ± 1.3	7.03	7.08	0.21
7.4	$P(DEA_{76}\text{-}DPA_{24})$	33.5 ± 1.8	0.14	-0.8 ± 0.5	7.31	7.44	0.18

Table S5. Characterization of two representative nanoprobes in PBS and medium at pH 7.4 and 5.0.

Nanoprobe	Solution	pH	D_h (nm)	PDI	Zeta-potential (mV)
$P(DEA_{40}\text{-}D5A_{40})$	PBS	7.4	29.4 ± 3.4	0.12	-1.5 ± 2.2
		5.0	9.2 ± 0.4	-	4.4 ± 2.4
	Medium	7.4	33.2 ± 4.4	0.10	-1.1 ± 0.7
		5.0	n.d.[a]	n.d.[a]	14.6 ± 2.6
$P(DPA_{40}\text{-}DBA_{40})$	PBS	7.4	36.3 ± 2.4	0.24	0.4 ± 0.7
		5.0	7.3 ± 0.7	-	9.8 ± 2.8
	Medium	7.4	36.8 ± 3.1	0.21	-1.1 ± 0.3
		5.0	n.d.[a]	n.d.[a]	13.4 ± 1.1

[a] Not detected due to the interference from serum proteins.

Table S6. Measurement of conjugation efficiency and quantum yields of dye-conjugated **PDPA** polymers.

Dyes	Dye conjugation		Quantum yield (Φ_F)[a]		
	Number	Efficiency (%)	Free dye[b]	Conjugated dye	Mixture[d]
Marina Blue	2.1	71	0.89	0.73	0.87
BODIPY 493/503	2.0	68	0.90	0.10/0.87[c]	0.86
TMR	2.2	72	0.68	0.15	0.64
Cy5	2.0	68	0.28	0.28	0.28

[a] In methanol unless noted otherwise. [b] Obtained from literature. [c] In methanol with 0.5% 1 M HCl. [d] Mixture of free dye with dye-free PDPA copolymer.

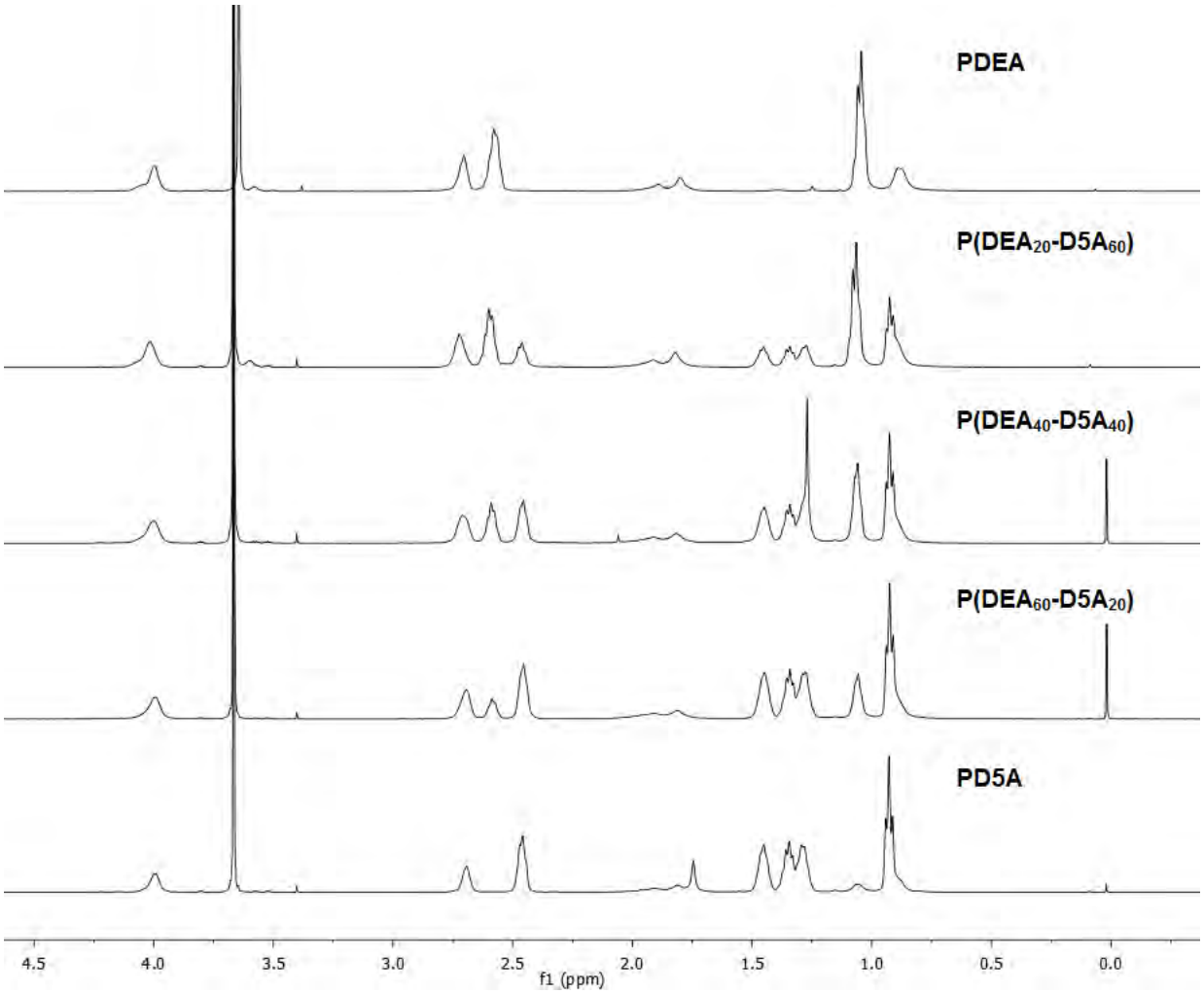

Figure S1. ^{1}HNMR spectra of **PEO-P(DEA$_x$-D5A$_y$)** (x + y = 80) copolymers at different monomer (DEA-MA and D5A-MA) ratios in the random copolymers. The peaks at 0.9 ppm and 1.1 ppm were used to estimate the monomer composition in the hydrophobic PR block.

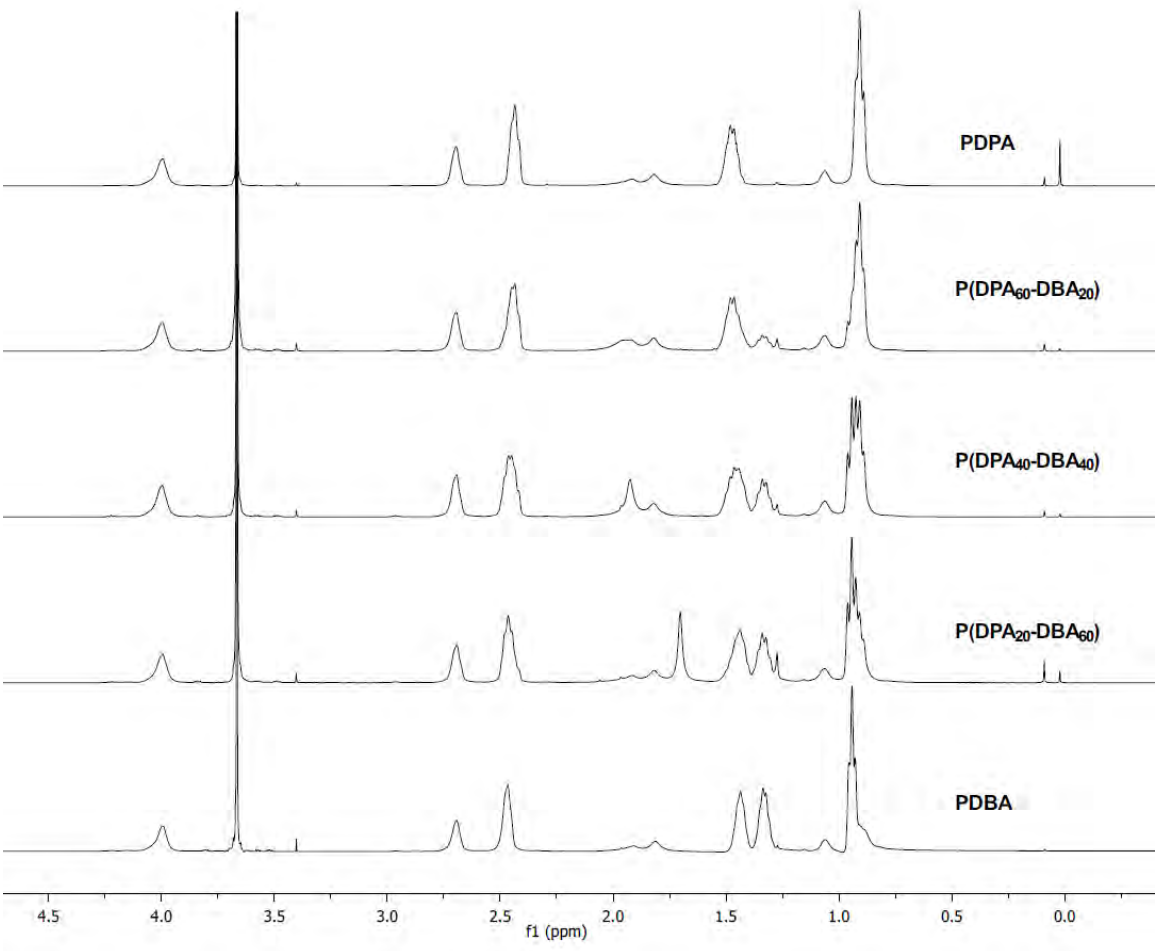

Figure S2. ^{1}HNMR spectra of **PEO-P(DPA$_x$-DBA$_y$)** (x + y = 80) copolymers at different monomer (DPA-MA and DBA-MA) ratios in the random copolymers. The peaks at 1.3 ppm and 1.4 ppm were used to estimate the monomer composition in the hydrophobic PR block.

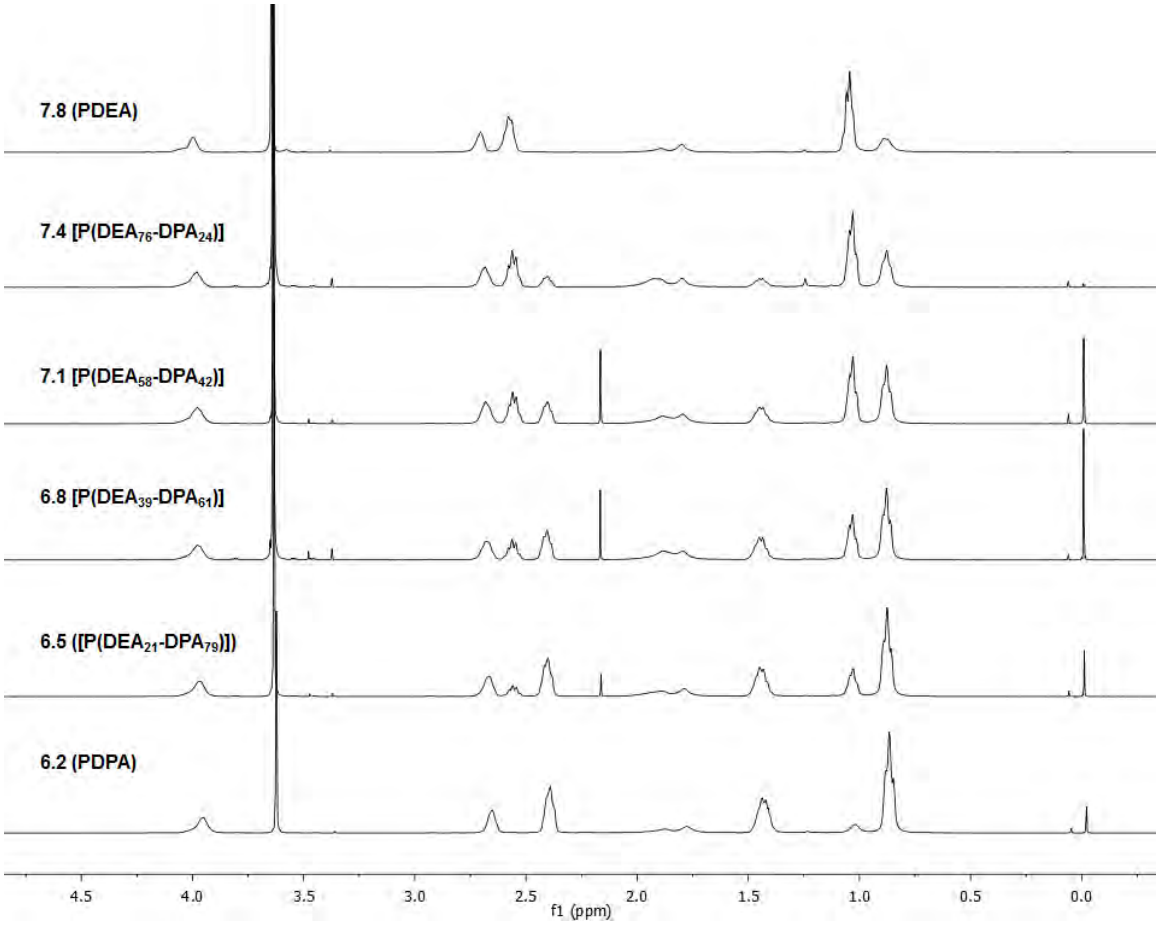

Figure S3. [1]HNMR spectra of nanoprobe compositions with pH_t values at 7.8, 7.4, 7.1, 6.8, 6.5 and 6.2 by adjusting the monomer (DEA-MA and DPA-MA) ratios in the hydrophobic PR block. The peaks at 0.9 ppm and 1.0-1.1 ppm were used to estimate the monomer composition in the hydrophobic PR block.

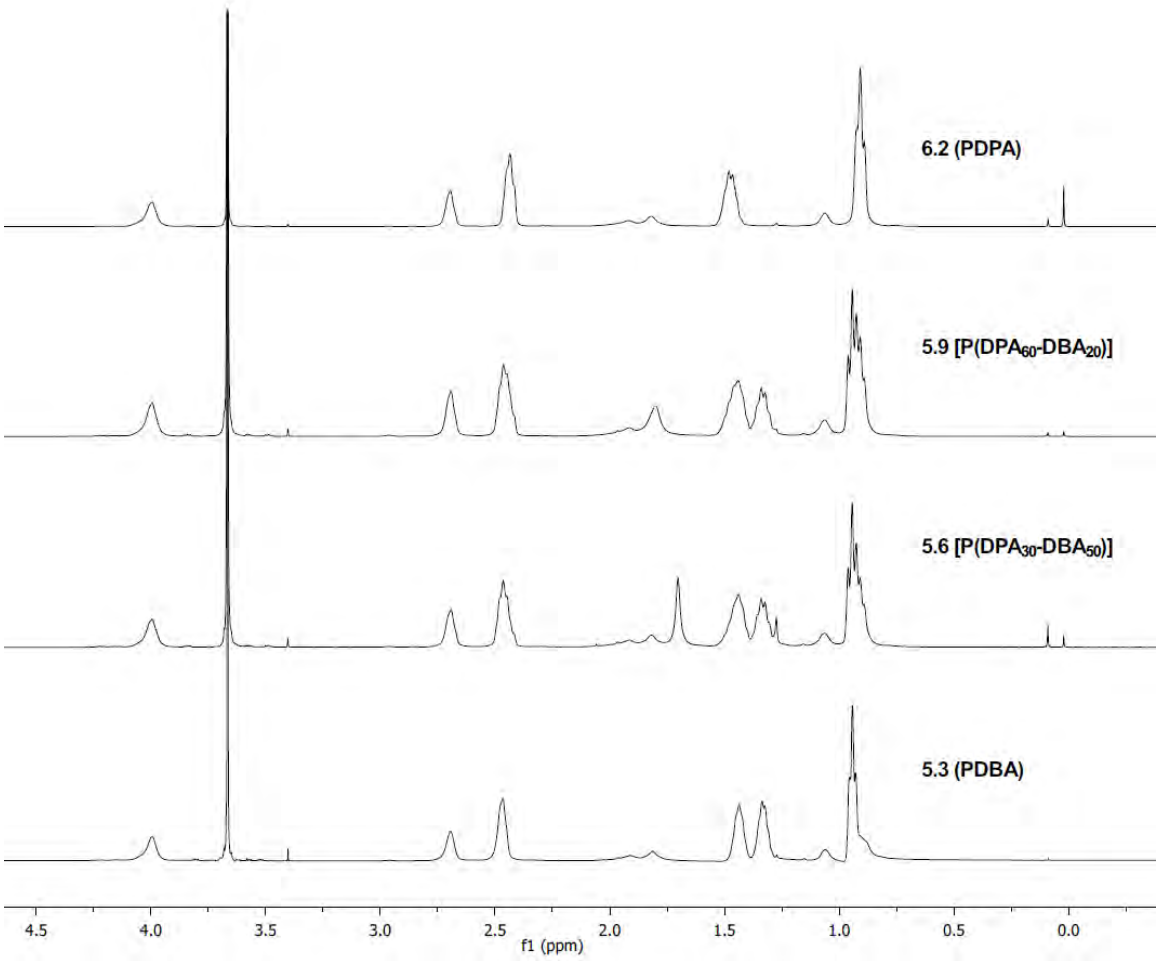

Figure S4. ^{1}HNMR spectra of nanoprobe compositions with pH_t values at 6.2, 5.9, 5.6 and 5.3 by adjusting the monomer (DPA-MA and DBA-MA) ratios in the hydrophobic PR block. The peaks at 1.3 ppm and 1.4 ppm were used to estimate the monomer composition in the hydrophobic PR block.

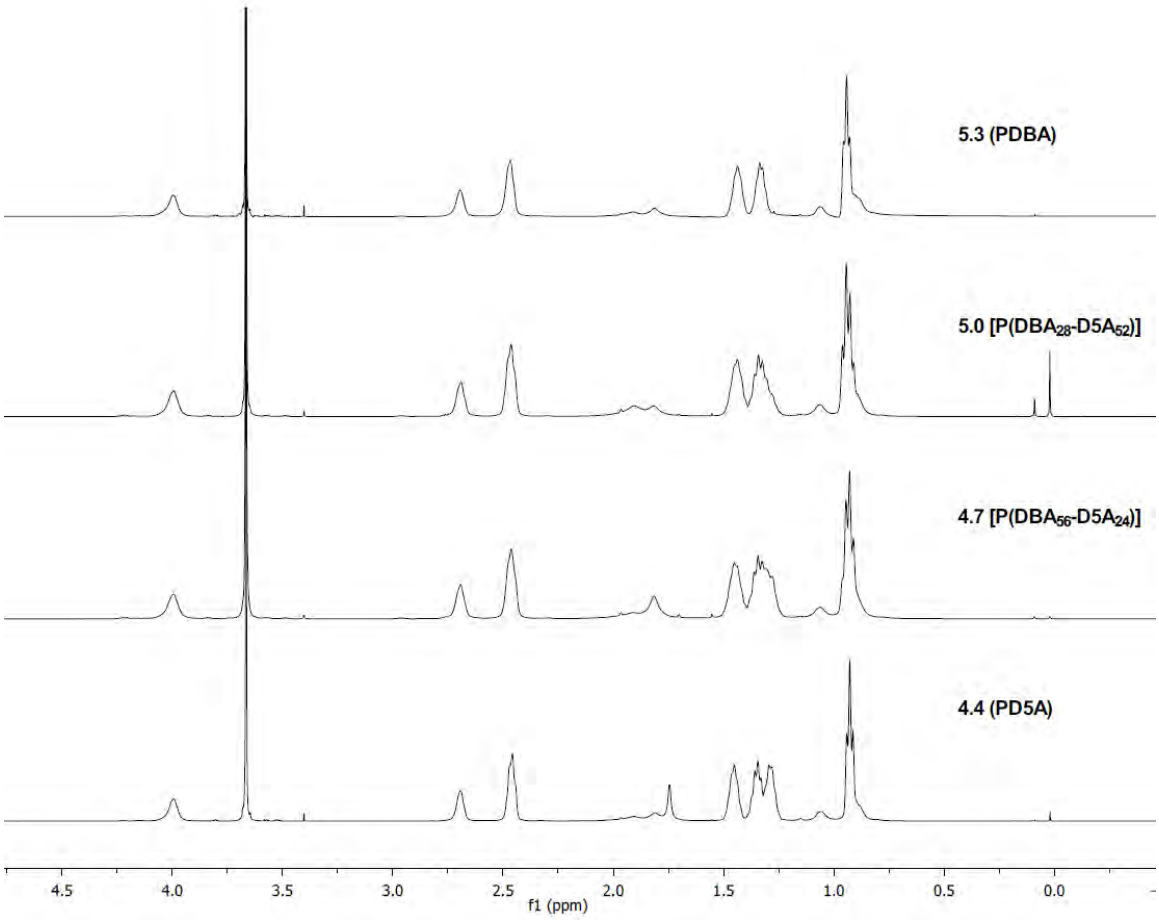

Figure S5. [1]HNMR spectra of nanoprobe compositions with pH_t values at 5.3, 5.0, 4.7 and 4.4 by adjusting the monomer (DBA-MA and D5A-MA) ratios in the hydrophobic PR block. The peaks at 1.3 ppm and 1.4 ppm were used to estimate the monomer composition in the hydrophobic PR block.

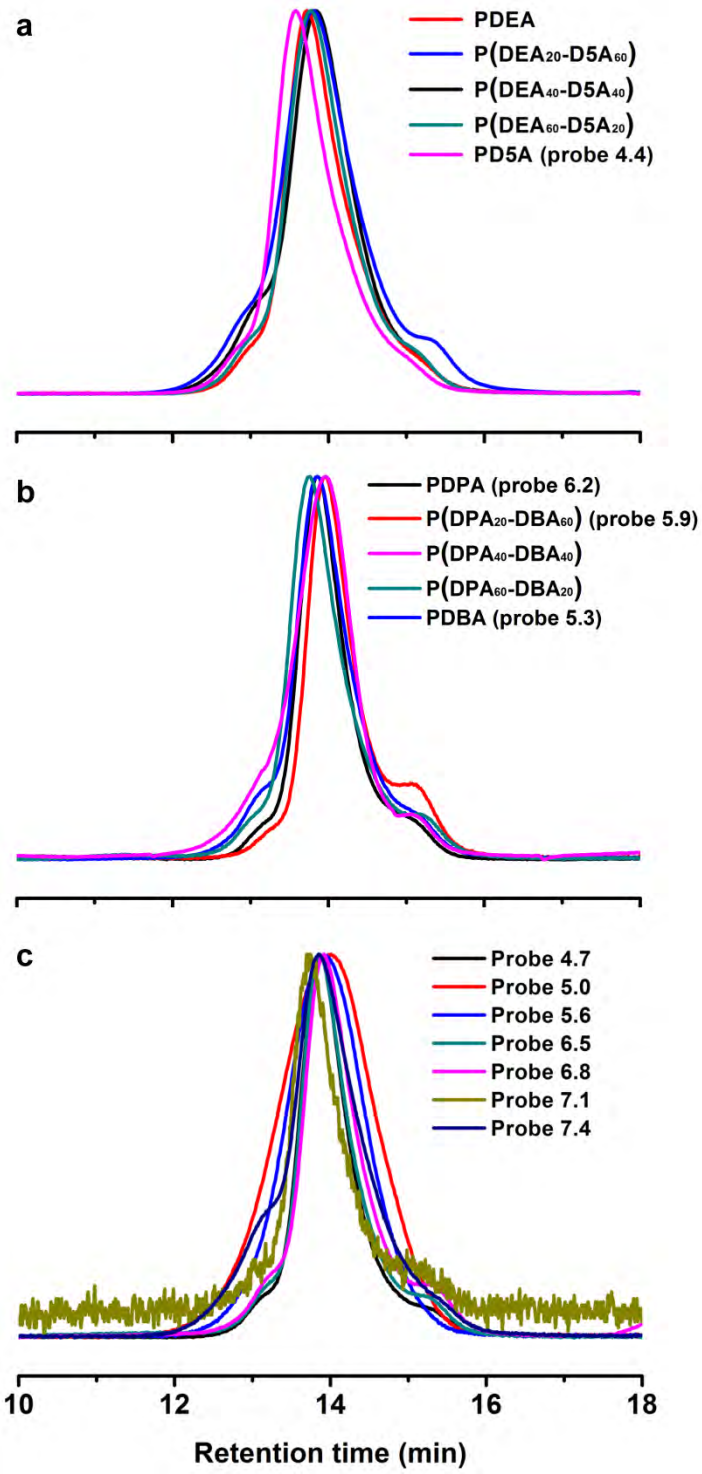

Figure S6. GPC chromatograms of all the copolymers. (**a**) P(DEA$_x$-D5A$_y$) series; (**b**) P(DPA$_x$-DBA$_y$) series; and (**c**) nanoprobes 4.7, 5.0, 5.6, 6.5, 6.8, 7.1 and 7.4.

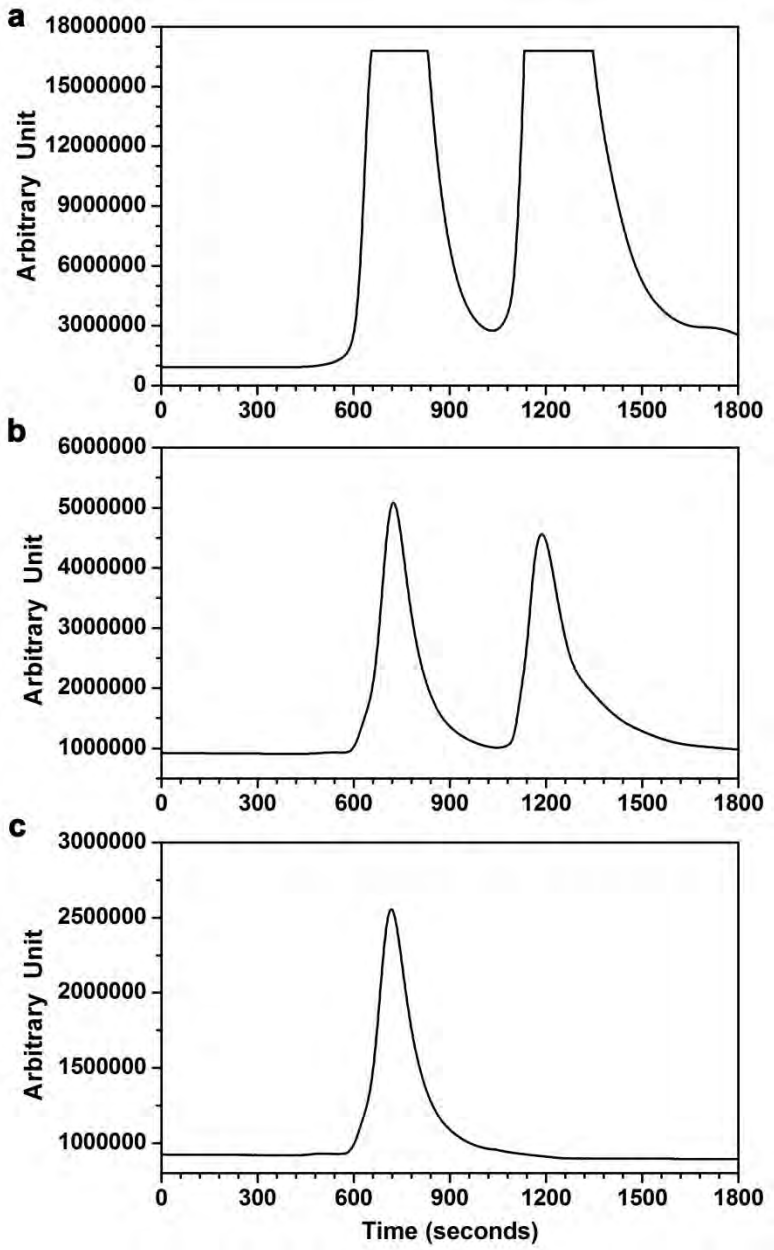

Figure S7. GPC chromatograms for the purification of dye-conjugated polymers. (**a**) Representative preparative GPC of **PDPA-TMR** synthetic mixture during purification (peak at elution time 700s is from PDPA-TMR and peak at 1200s is from the free TMR). Polymer fraction (600-900 s) was collected. (**b**) Analytical GPC of low concentration of **PDPA-TMR** synthetic mixture. (**c**) Analytical GPC of purified **PDPA-TMR** polymer showing the complete removal of free dye.

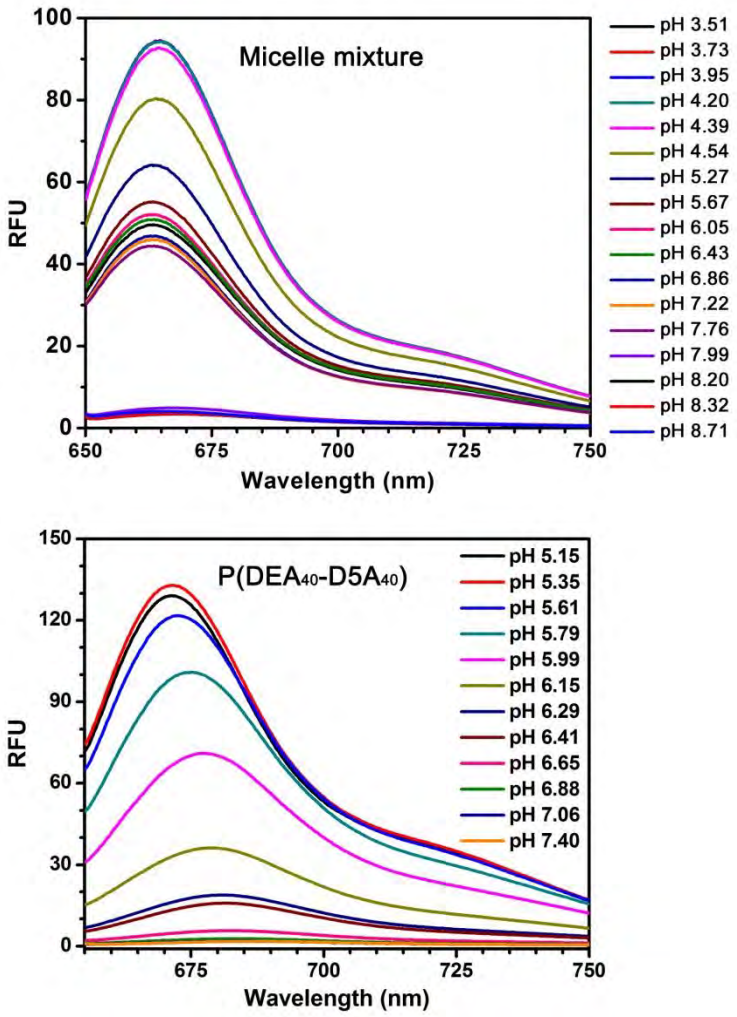

Figure S8. pH-dependent fluorescence spectra of **PDEA/PD5A** micelle mixture vs. **P(DEA$_{40}$-D5A$_{40}$)** copolymer nanoprobes. Cy5 dye ($\lambda_{ex}/\lambda_{em}$ = 646/662 nm) was conjugated to the PR blocks of the corresponding copolymers. The normalized fluorescence intensity vs. pH relationships were shown in **Figure 3a** in the main text.

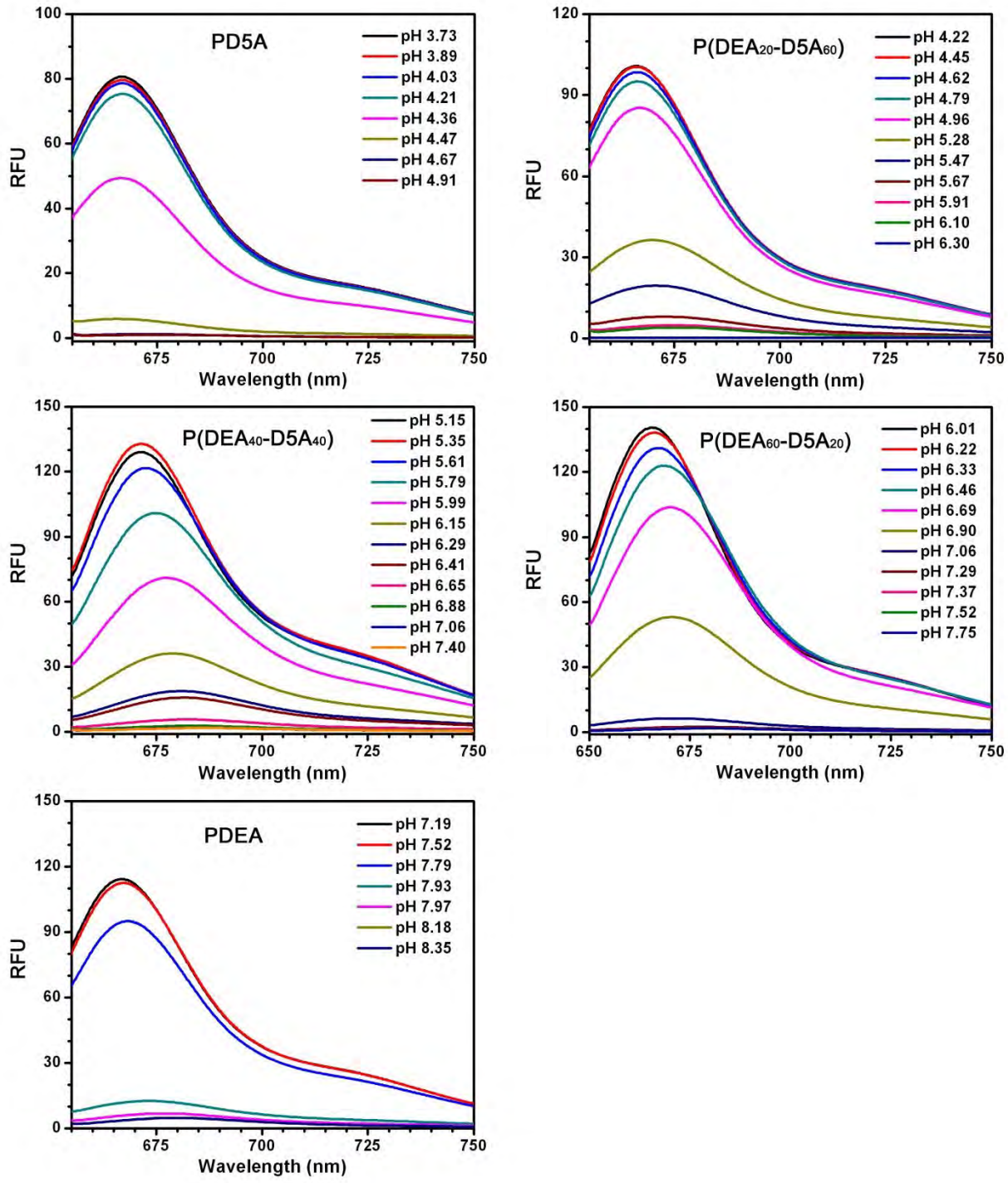

Figure S9. pH-dependent fluorescence spectra of coarse-tuned **P(DEA$_x$-D5A$_y$)** nanoprobes. Cy5 dye ($\lambda_{ex}/\lambda_{em}$ = 646/662 nm) was conjugated to the PR blocks of the copolymers. The normalized fluorescence intensity vs. pH relationships were shown in **Figure 3b** in the main text.

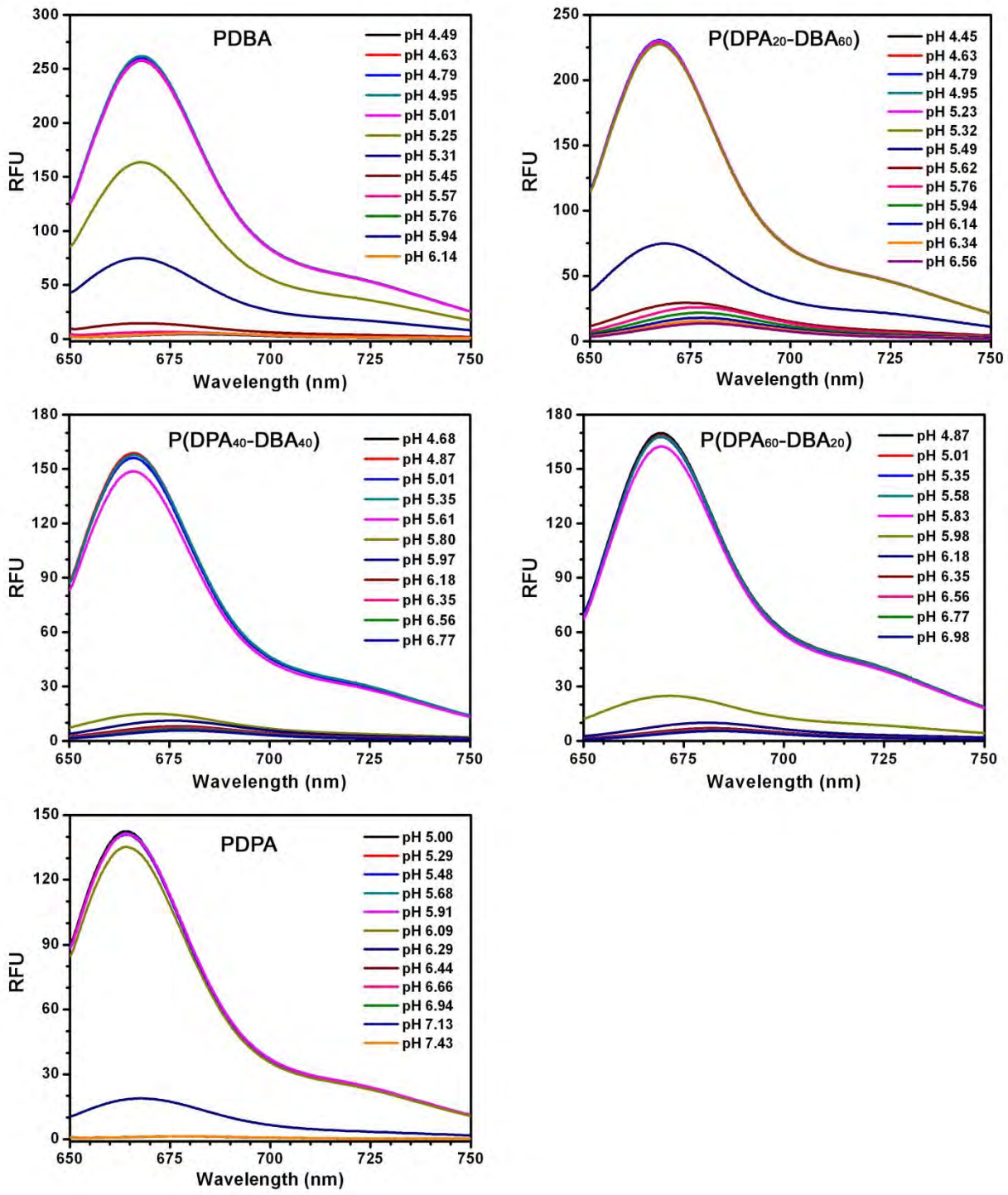

Figure S10. pH-dependent fluorescence spectra of fine-tuned **P(DPA$_x$-DBA$_y$)** nanoprobes. Cy5 dye ($\lambda_{ex}/\lambda_{em}$ = 646/662 nm) was conjugated to the PR blocks of the copolymers. The normalized fluorescence intensity vs. pH relationships were shown in **Figure 4a** in the main text.

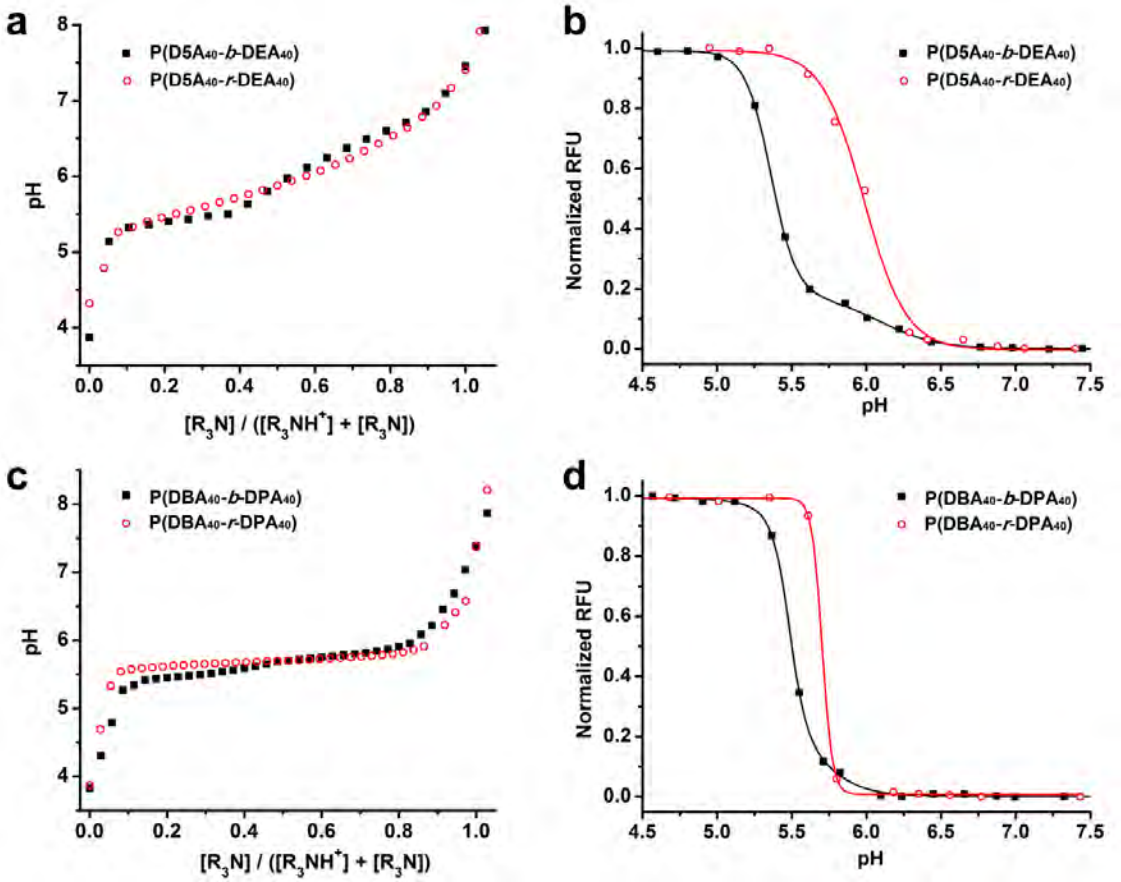

Figure S11. Comparison of the pH-responsive properties of two representative triblock copolymers with diblock copolymers with random PR segments. (**a**) pH titration curves for **P(D5A$_{40}$-*b*-DEA$_{40}$)** and **P(D5A$_{40}$-*r*-DEA$_{40}$)** copolymers as a function of molar fraction of tertiary amino groups. (**b**) Normalized fluorescence intensity as a function of pH for Cy5-conjugated **P(D5A$_{40}$-*b*-DEA$_{40}$)** and **P(D5A$_{40}$-*r*-DEA$_{40}$)** nanoprobes. (**c**) pH titration curves for **P(DBA$_{40}$-*b*-DPA$_{40}$)** and **P(DBA$_{40}$-*r*-DPA$_{40}$)** copolymers as a function of molar fraction of tertiary amino groups. (**d**) Normalized fluorescence intensity as a function of pH for Cy5-conjugated **P(DBA$_{40}$-*b*-DPA$_{40}$)** and **P(DBA$_{40}$-*r*-DPA$_{40}$)** nanoprobes.

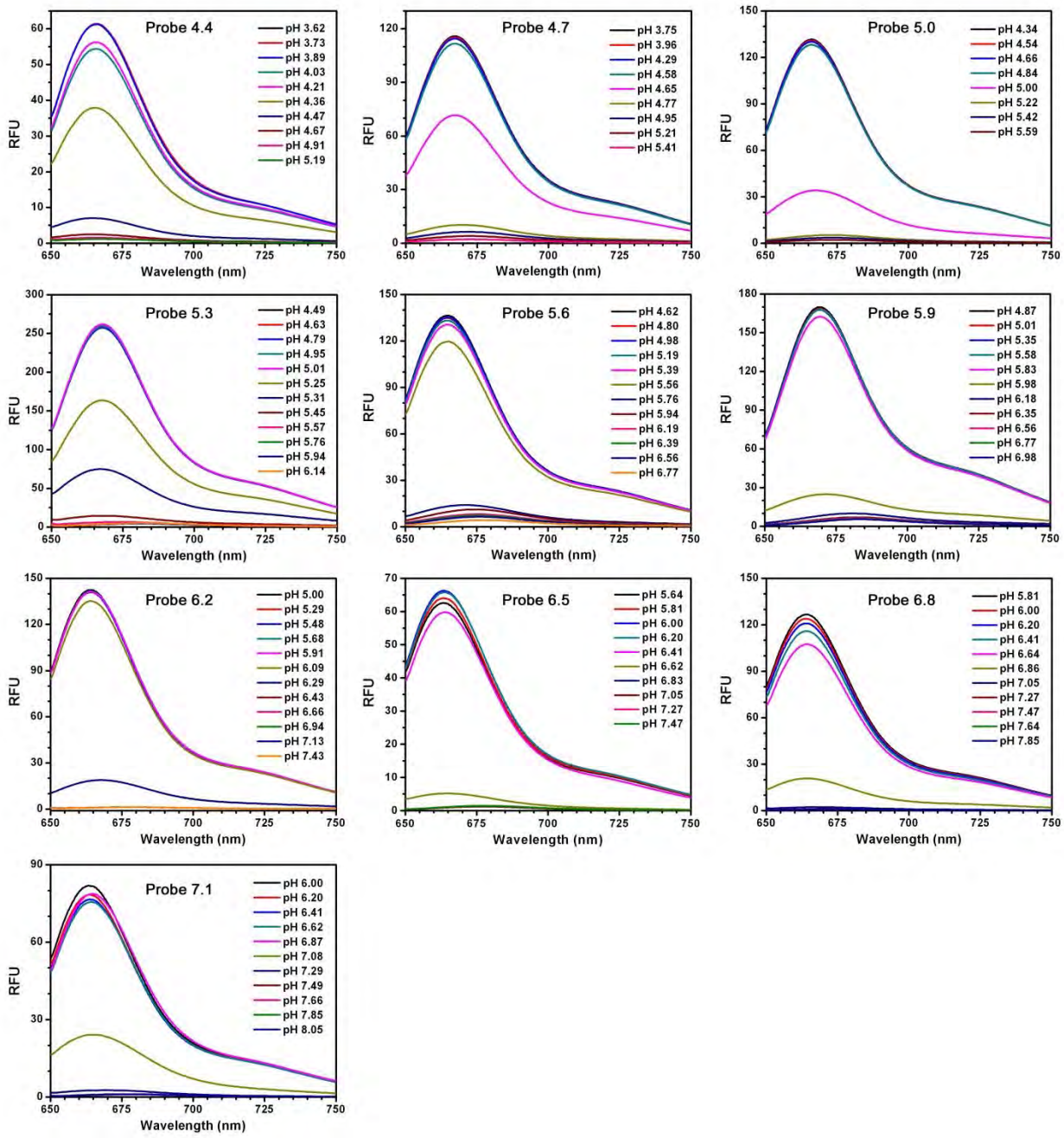

Figure S12. pH-dependent fluorescence spectra of the UPS library nanoprobes. The composition for each UPS nanoprobe was shown in Table S3. Cy5 dye ($\lambda_{ex}/\lambda_{em}$ = 646/662 nm) was conjugated to the PR blocks of the copolymers. The normalized fluorescence intensity vs. pH relationships were shown in **Figure 4d** in the main text.

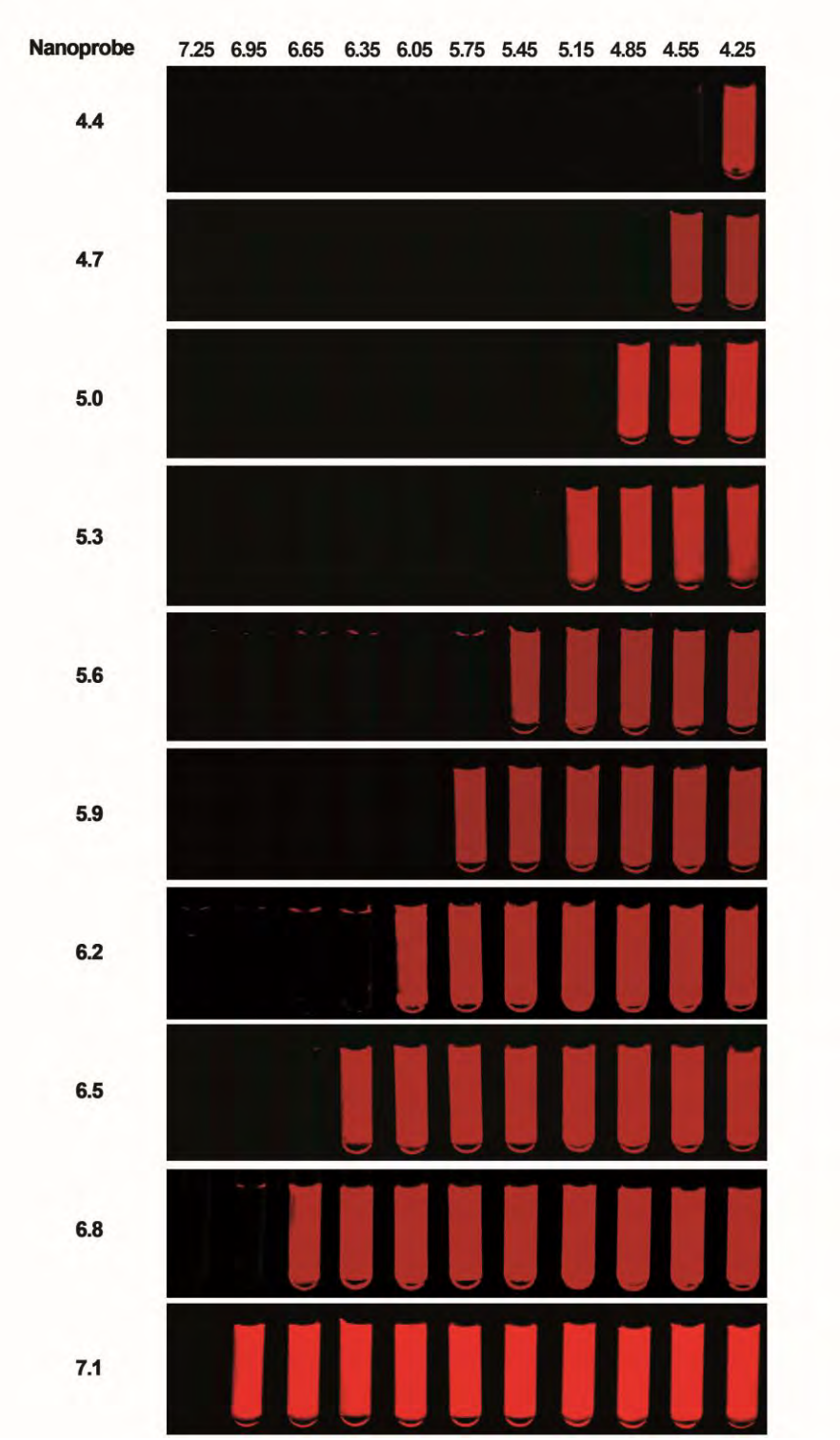

Figure S13. Fluorescence imaging of the UPS library consisting of 10 nanoprobes with 0.3 pH increment. The composition for each UPS nanoprobe was shown in Table S3. Cy5 dye ($\lambda_{ex}/\lambda_{em}$ = 646/662 nm) was conjugated to the PR blocks of the copolymers. Images of the nanoprobes were taken on a Maestro Imaging system.

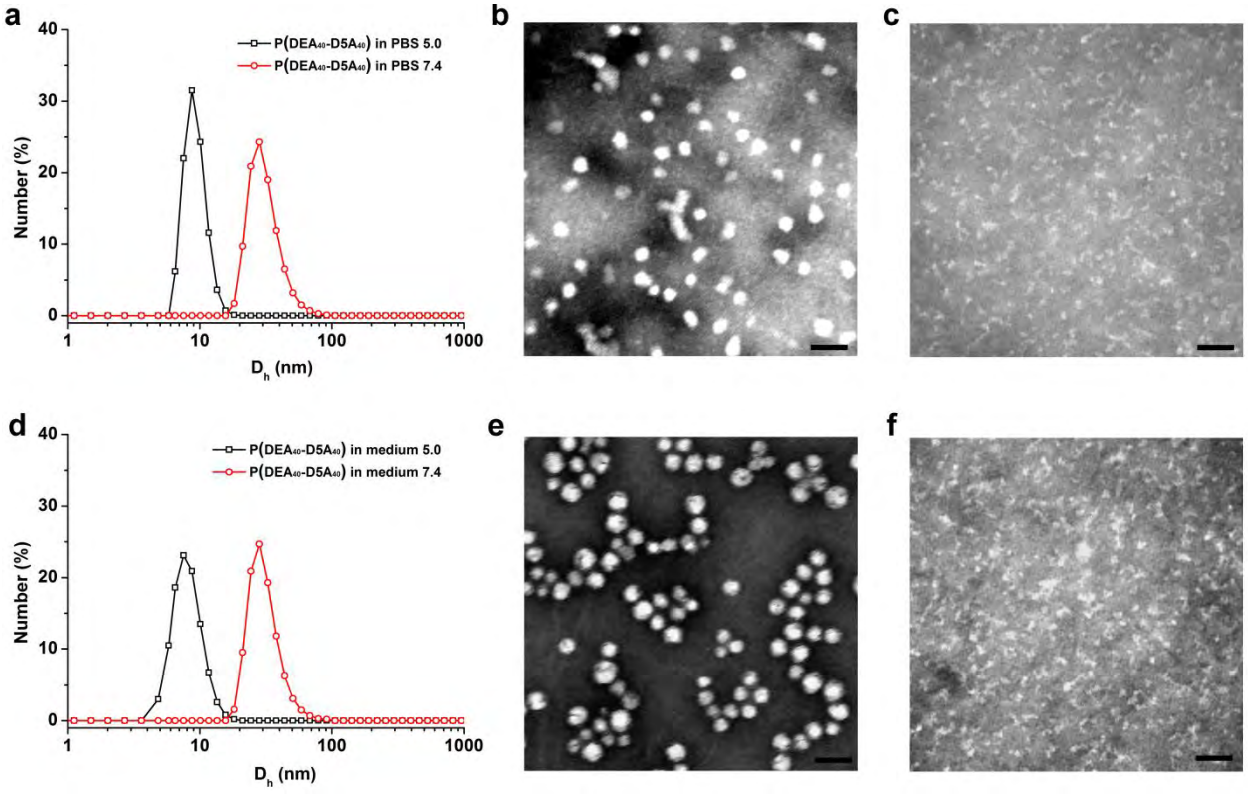

Figure S14. Characterization of **P(DEA$_{40}$-D5A$_{40}$)** nanoprobes. (**a**) DLS histograms of **P(DEA$_{40}$-D5A$_{40}$)** nanoprobes as micelles in pH 7.4 PBS solution and as unimers in pH 5.0 PBS solution. (**b, c**) TEM image of **P(DEA$_{40}$-D5A$_{40}$)** nanoprobes from pH 7.4 and 5.0 solutions, respectively. Scale bars = 50 nm. (**d**) DLS histograms of **P(DEA$_{40}$-D5A$_{40}$)** nanoprobes as micelles in pH 7.4 and as unimers in pH 5.0 solution of cell culture medium containing 10% FBS. (**e, f**) TEM image of **P(DEA$_{40}$-D5A$_{40}$)** nanoprobes in pH 7.4 and pH 5.0 solutions of cell culture medium containing 10% FBS, respectively. Scale bars = 50 nm.

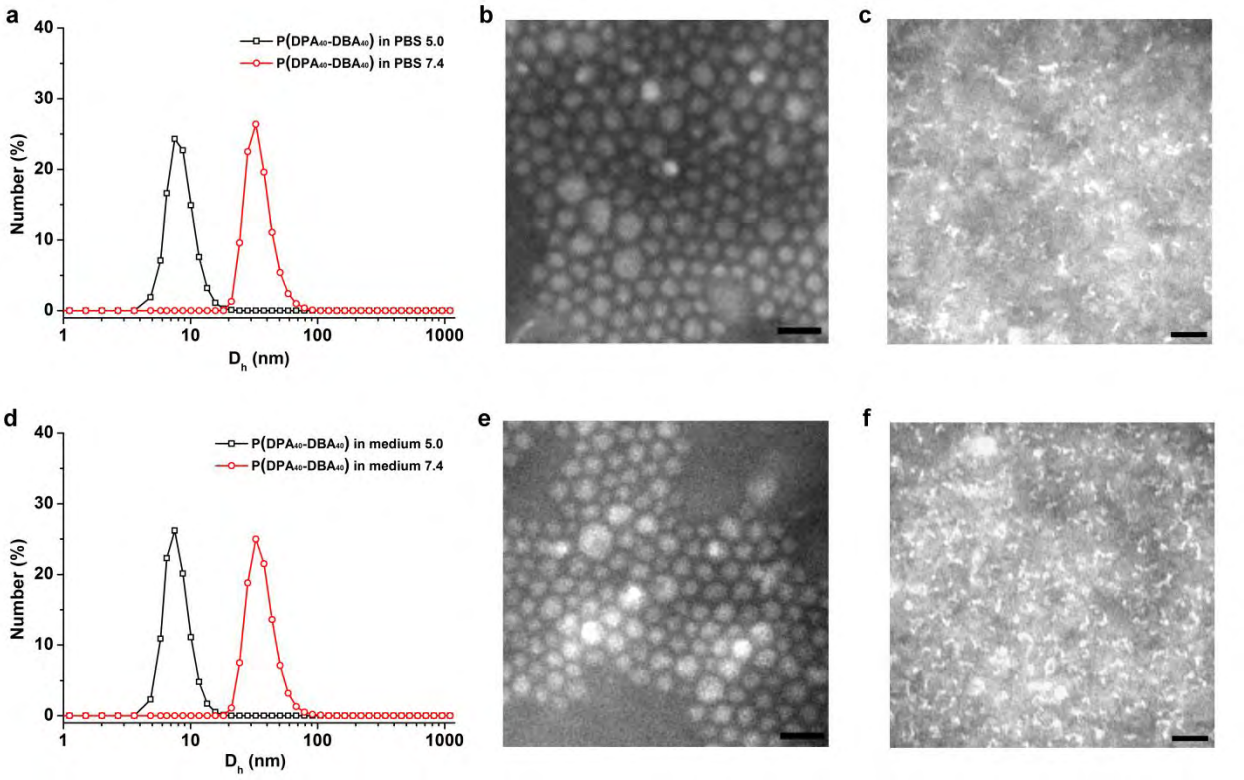

Figure S15. Characterization of **P(DPA$_{40}$-DBA$_{40}$)** nanoprobes. (**a**) DLS histograms of **P(DPA$_{40}$-DBA$_{40}$)** nanoprobes as micelles in pH 7.4 PBS solution and as unimers in pH 5.0 PBS solution. (**b, c**) TEM image of **P(DPA$_{40}$-DBA$_{40}$)** nanoprobes from pH 7.4 and 5.0 solutions, respectively. Scale bars = 50 nm. (**d**) DLS histograms of **P(DPA$_{40}$-DBA$_{40}$)** nanoprobes as micelles in pH 7.4 and as unimers in pH 5.0 solution of cell culture medium containing 10% FBS. (**e, f**) TEM image of **P(DPA$_{40}$-DBA$_{40}$)** nanoprobes in pH 7.4 and pH 5.0 solutions of cell culture medium containing 10% FBS, respectively. Scale bars = 50 nm.

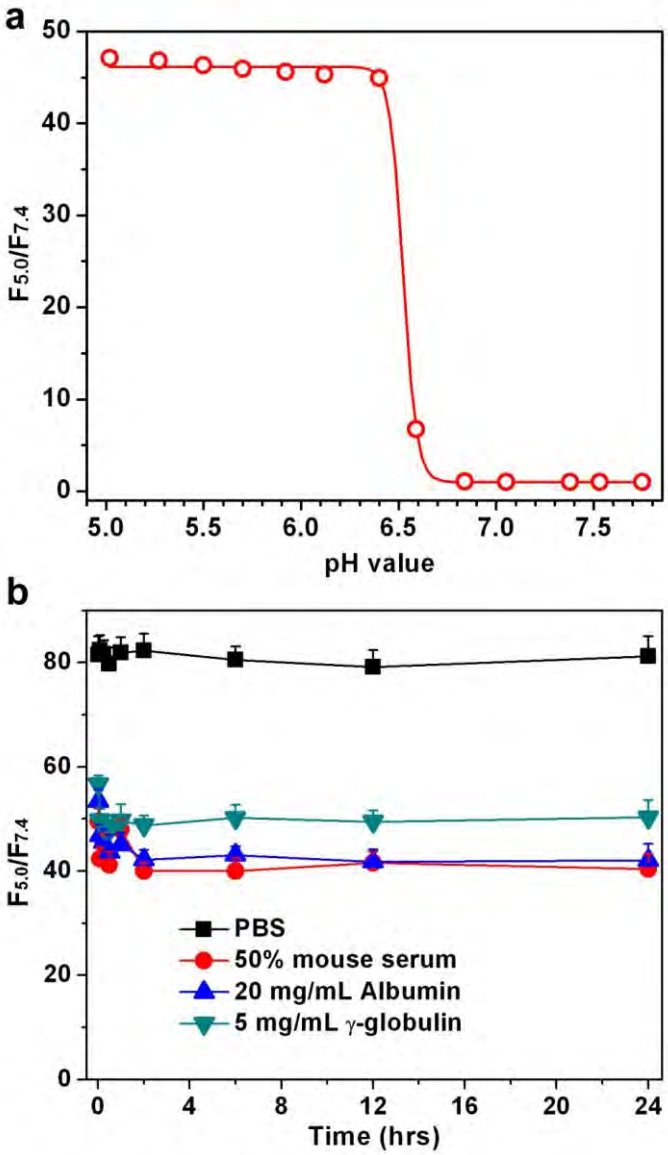

Figure S16. Evaluation of stability of nanoprobes under serum conditions. (**a**) Fluorescence ratio as a function of pH for **6.5-TMR** (**P(DEA$_{21}$-DPA$_{79}$)**) nanoprobe in the presence of 10% fetal bovine serum (FBS) in the cell culture medium. (**b**) Fluorescence on/off ratios of **6.5-TMR** nanoprobe in fresh mouse serum or solutions containing mouse serum components.

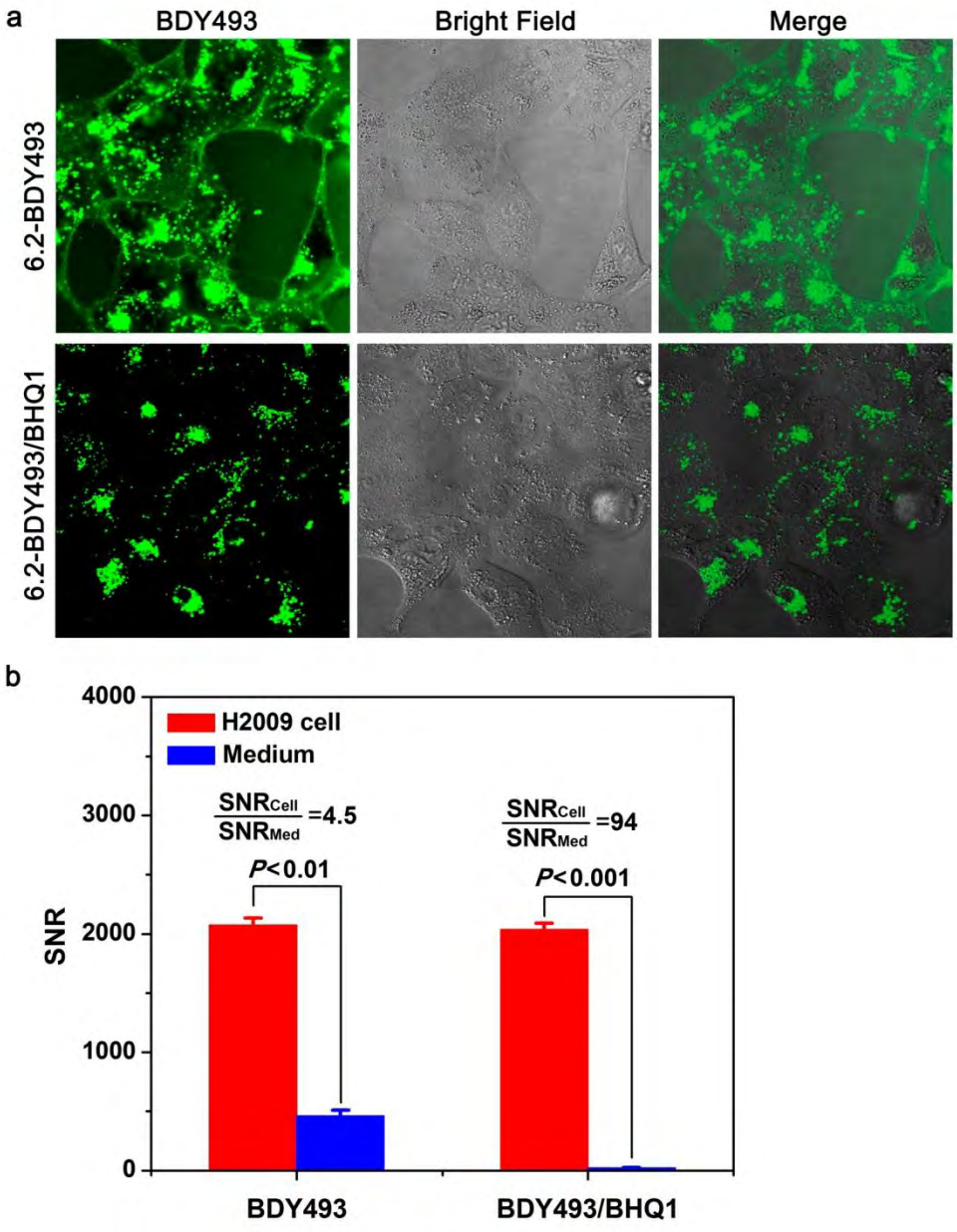

Figure S17. *In vitro* confocal imaging of H2009 lung cancer cells with **6.2-BDY493** and (**6.2-BDY493/BHQ1**) nanoprobes. (**a**) Representative confocal images of nanoprobes in H2009 cells. For the (**6.2-BDY493/BHQ1**) nanoprobes, the medium background signal is low and most nanoprobe signals come from activated nanoprobes in the acidic endosomes/lysosomes. (**b**) Quantitative analysis of signal to noise ratios (SNRs) of nanoprobes inside H2009 cells and medium background for the **6.2-BDY493** and (**6.2-BDY493/BHQ1**) nanoprobes. *P*-values are calculated using the Student's t-test.

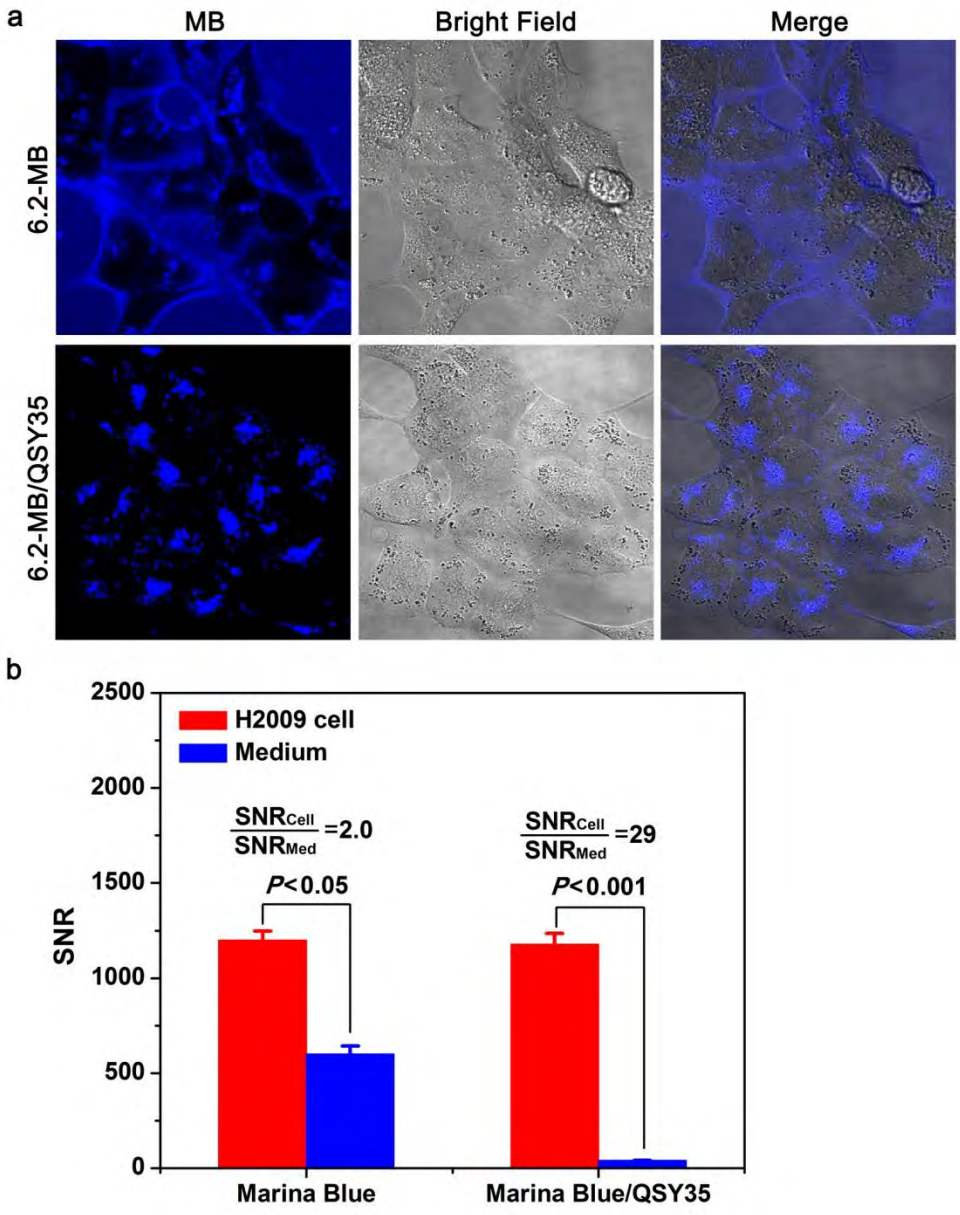

Figure S18. *In vitro* confocal imaging of H2009 lung cancer cells with **6.2-MB** and (**6.2-MB/QSY35**) nanoprobes. (**a**) Representative confocal images of nanoprobes in H2009 cells. For the (**6.2-MB/QSY35**) nanoprobes, the medium background signal is low and most nanoprobe signals come from activated nanoprobes in the acidic endosomes/lysosomes. (**b**) Quantitative analysis of signal to noise ratios (SNRs) of nanoprobes inside H2009 cells and medium background for the **6.2-MB** and (**6.2-MB/QSY35**) nanoprobes. *P*-values are calculated using the Student's t-test.

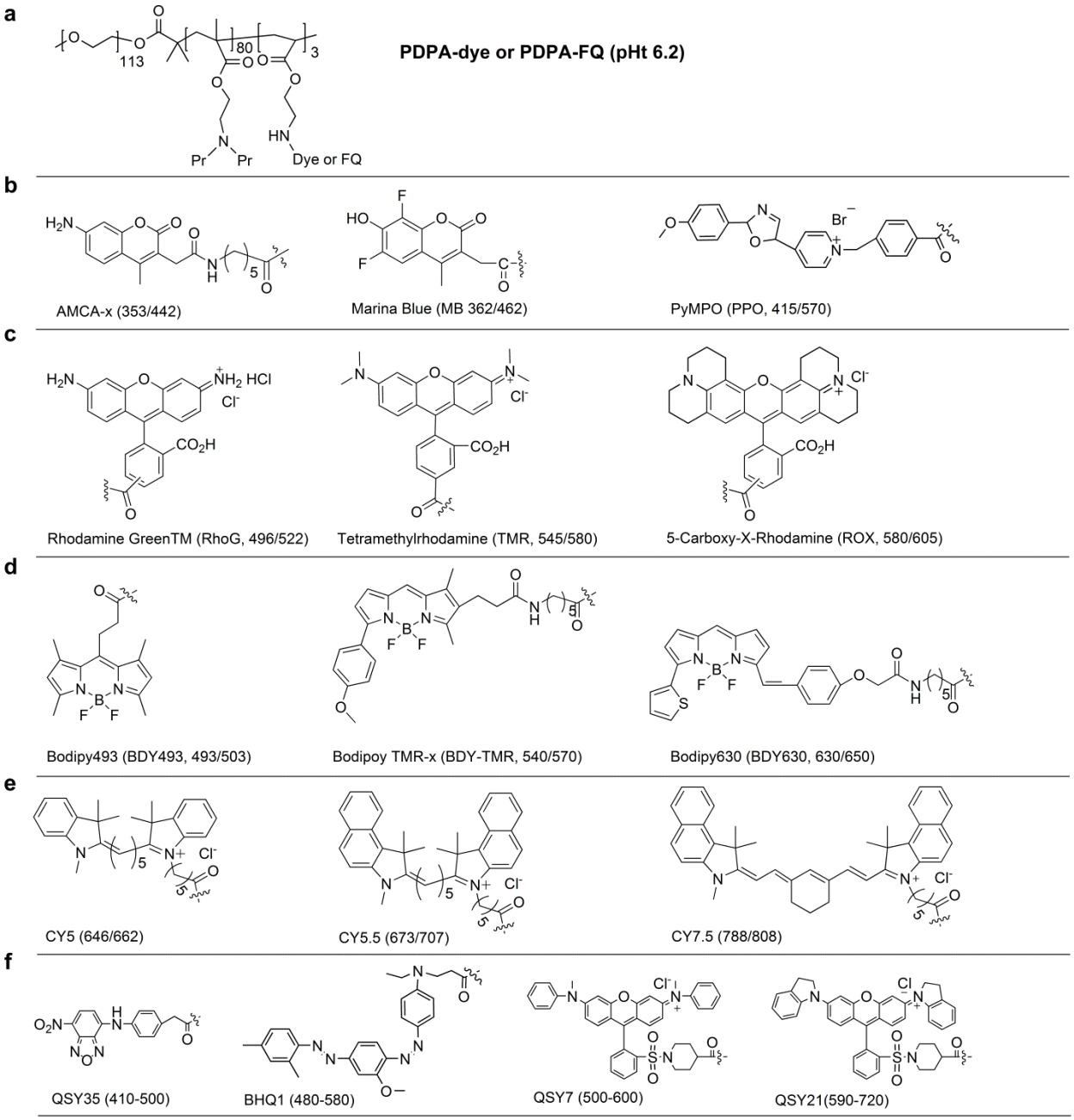

Figure S19. (**a**) Structures of the PEO-PDPA-Dye/FQ copolymers. (**b**)Structures of selected fluorophores with large Stokes shift. (**c**) Structures of selected Rhodamine dyes. (**d**) Structures of selected BODIPY dyes. (**e**) Structures of selected cyanine dyes. The excitation/emission wavelengths for all the fluorophores were shown in parenthesis in **b-e**, respectively. (**f**) Structures of the selected fluorescence quenchers. The active quenching range of each quencher was shown in parenthesis.

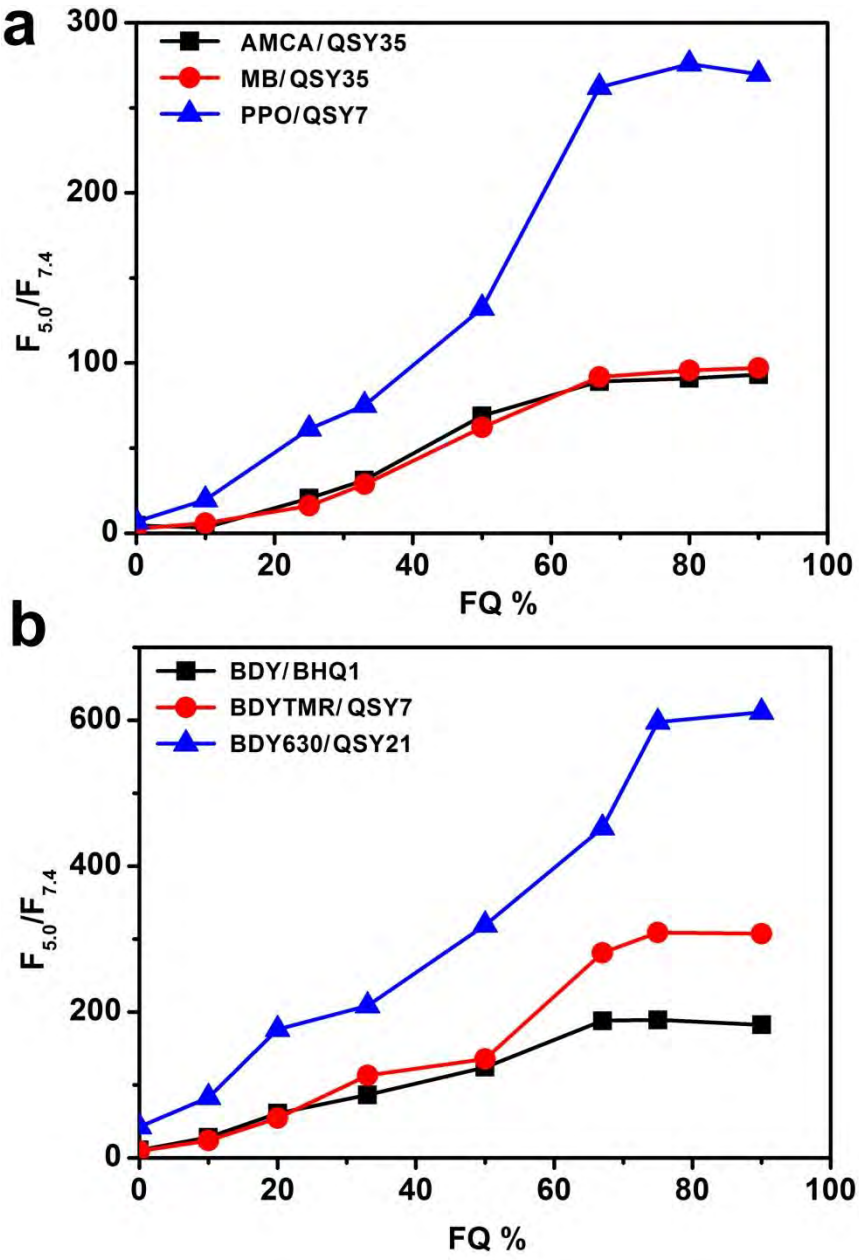

Figure S20. Fluorescence intensity ratios of mixed nanoparticles at pH 5.0 (ON) and pH 7.4 (OFF) at different ratios of (**PDPA-Dye**/**PDPA-FQ**). (**a**) Results for fluorophores with large Stokes shift (AMCA, MB and PPO). (**b**) Results for BODIPY families of fluorophores. The structures of the fluorophores and FQs were shown in **Figure S19**.

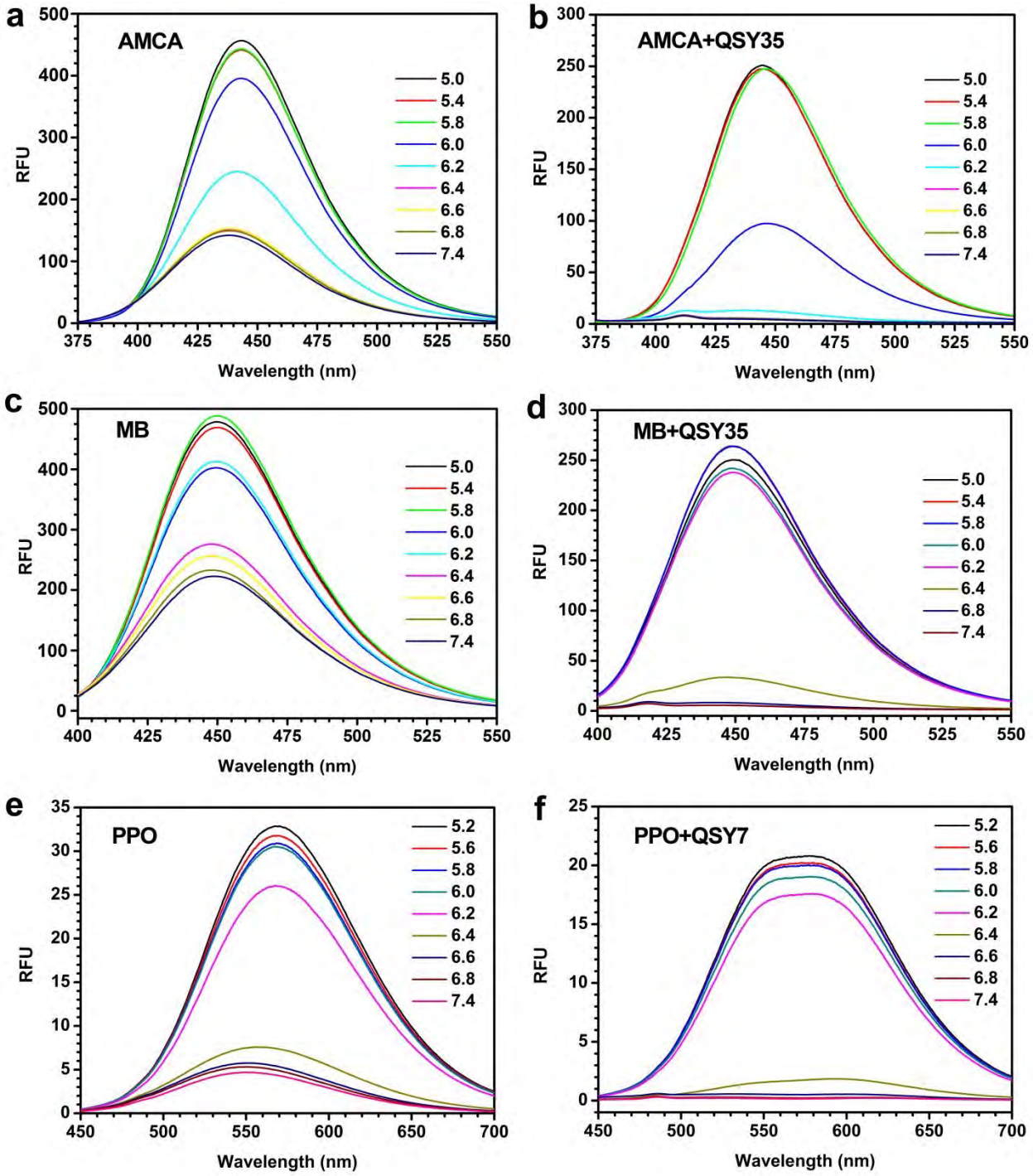

Figure S21. pH-dependent fluorescence spectra of nanoprobes without (left column) or with (right column) fluorescence quenchers. Fluorophores with large Stokes shift were presented in this study. The structures of the fluorophores and FQs were shown in **Figure S19**.

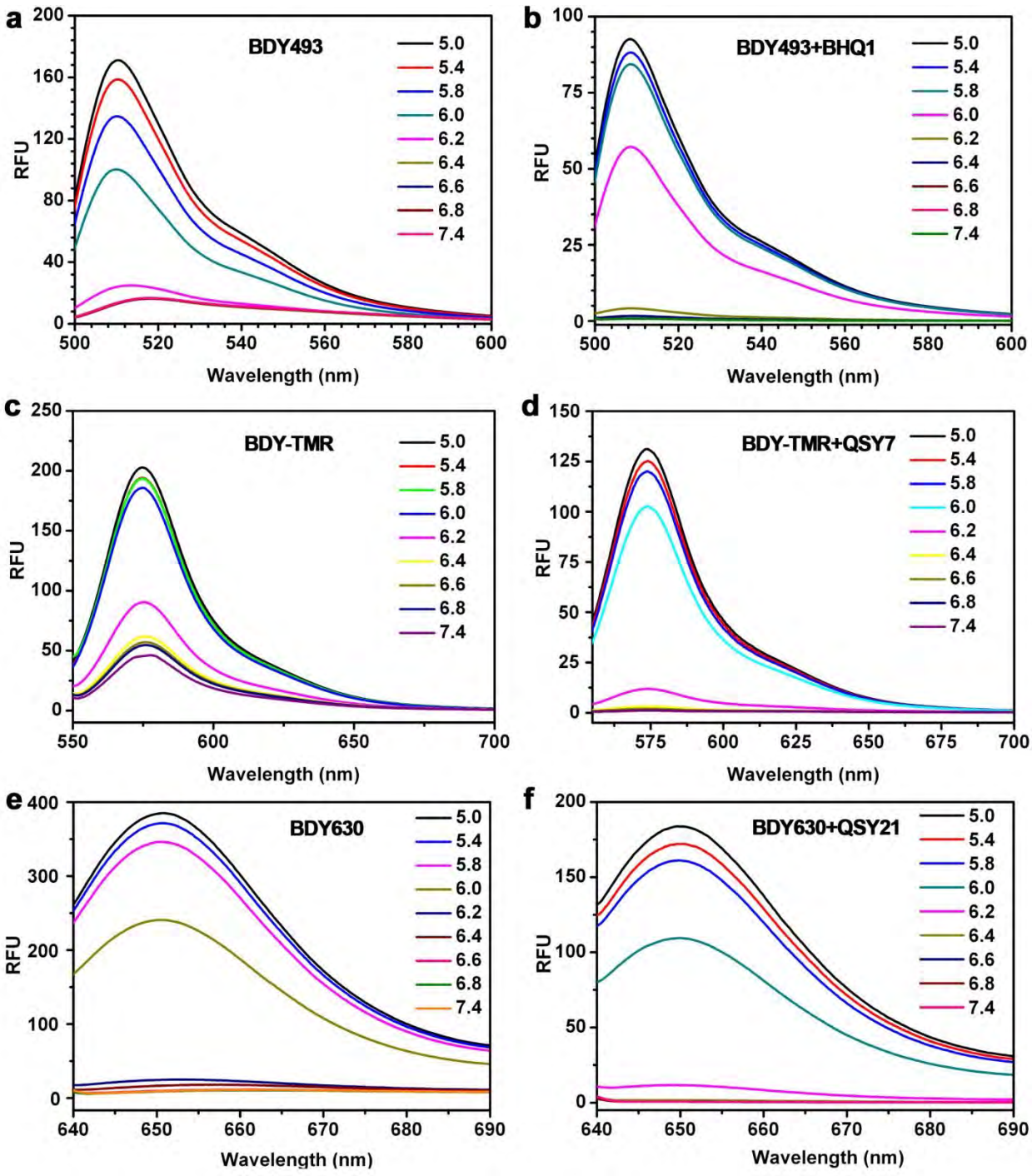

Figure S22. pH-dependent fluorescence spectra of nanoprobes without (left column) or with (right column) fluorescence quenchers. BODIPY family of fluorophores was presented in this study. The structures of the fluorophores and FQs were shown in **Figure S19**.

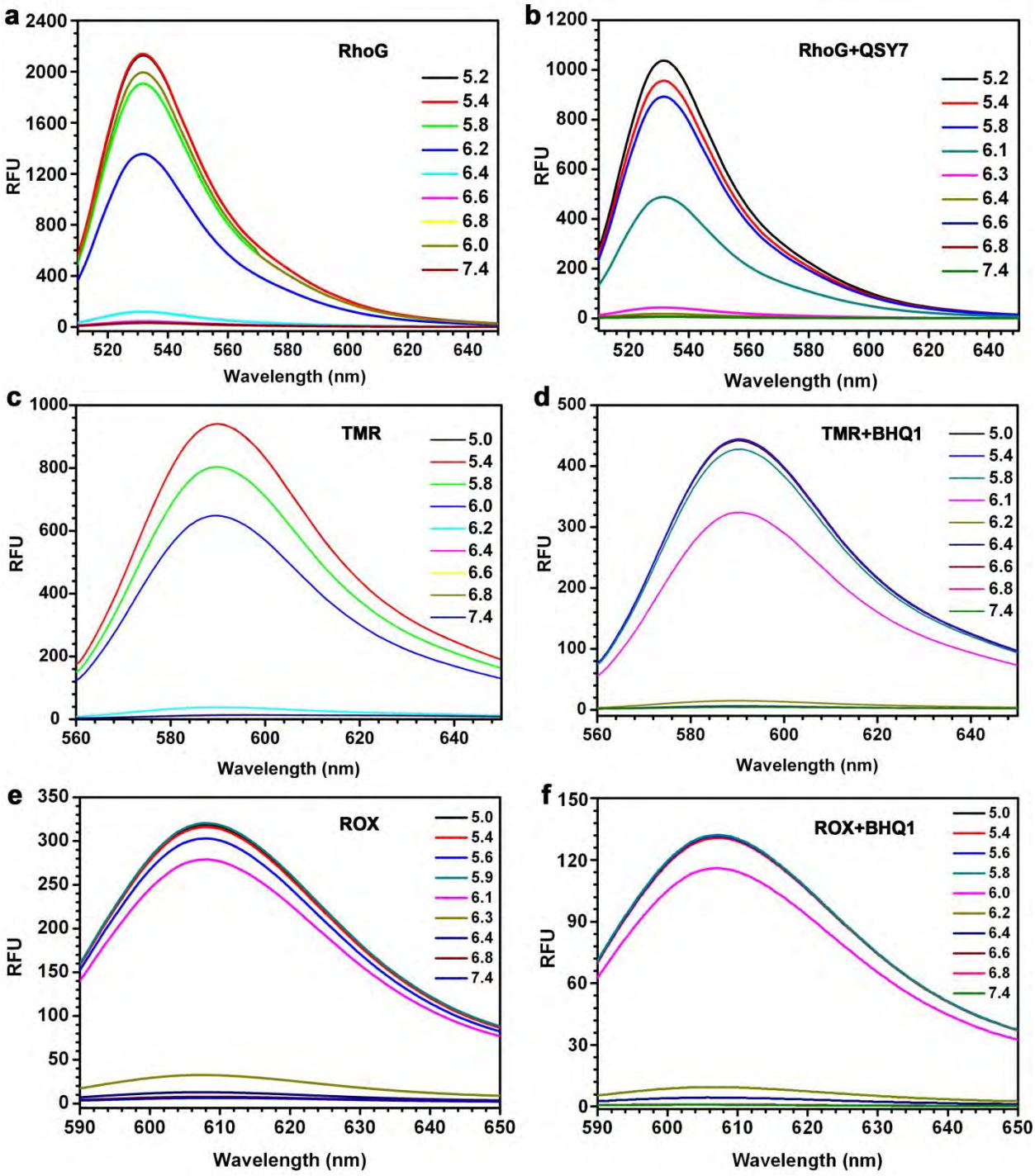

Figure S23. pH-dependent fluorescence spectra of nanoprobes without (left column) or with (right column) fluorescence quenchers. Rhodamine family of fluorophores was presented in this study. The structures of the fluorophores and FQs were shown in **Figure S19**.

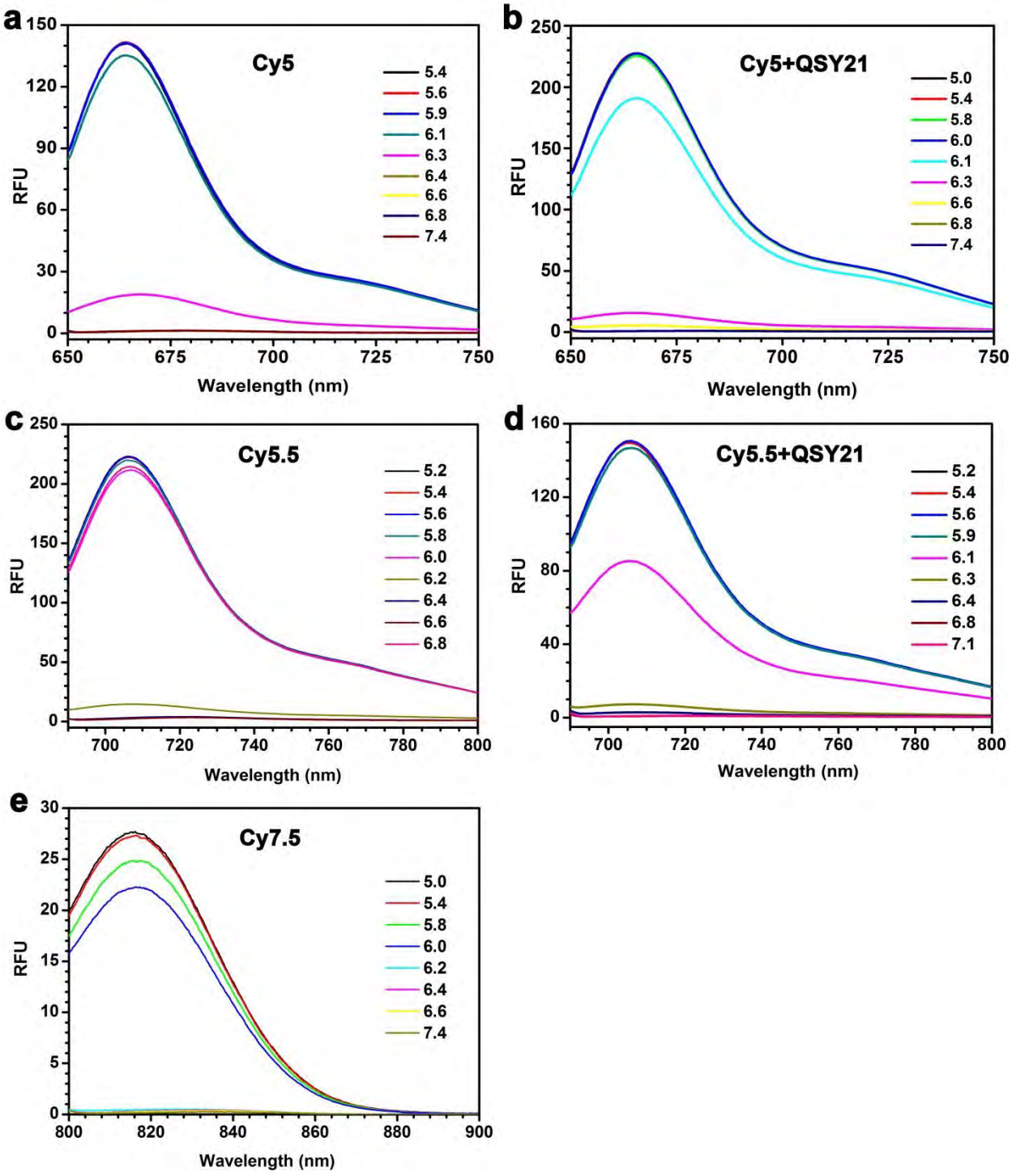

Figure S24. pH-dependent fluorescence spectra of nanoprobes without (left column) or with (right column) fluorescence quenchers. Cyanine family of fluorophores was presented in this study. The structures of the fluorophores and FQs were shown in **Figure S19**.

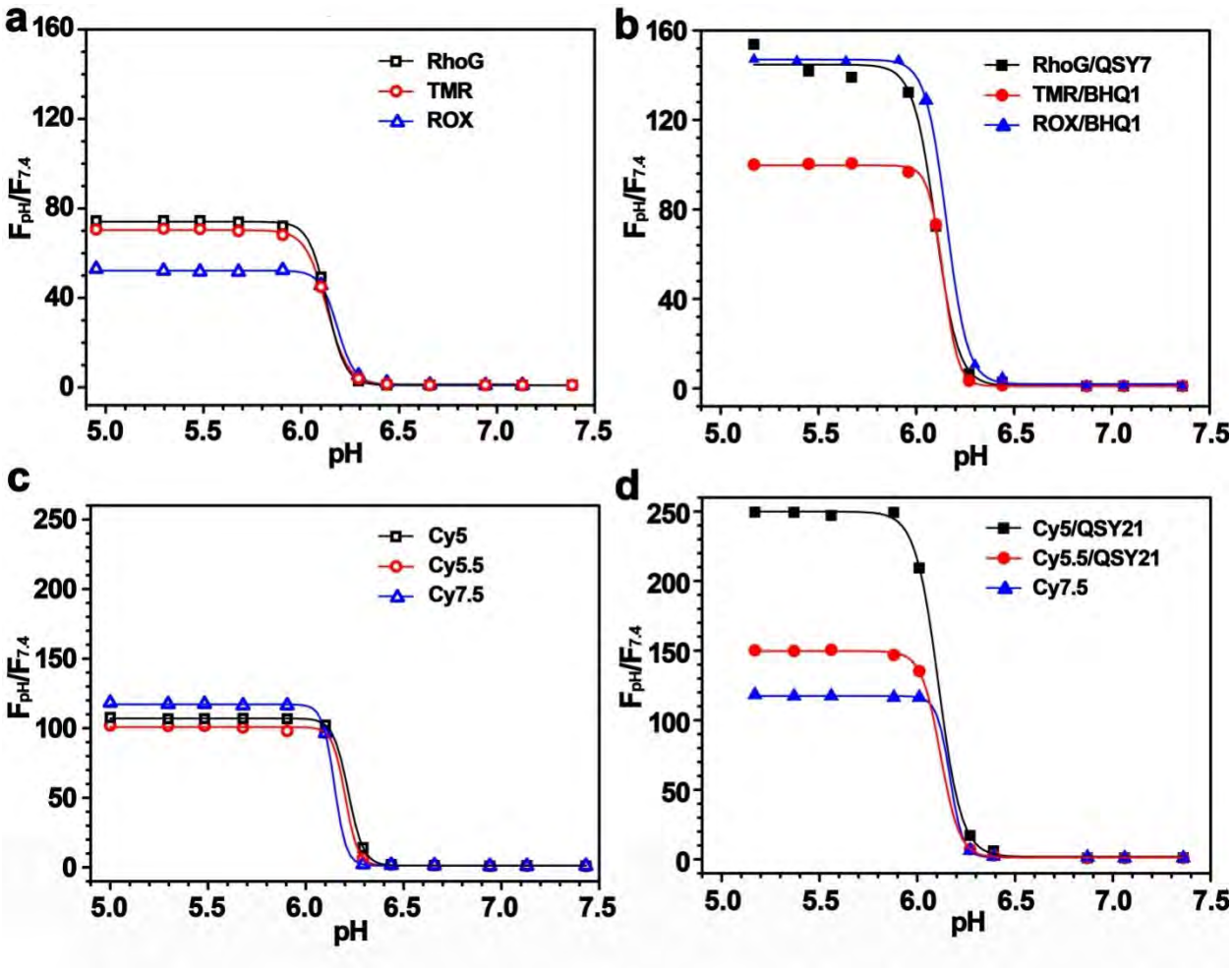

Figure S25. Fluorescence intensity ratio at different pH to pH 7.4 ($F_{pH}/F_{7.4}$) was plotted for copolymer alone (**a, c**) and with the addition of FQ-conjugated copolymers (**b, d**) for Rhodamine and Cyanine families of dyes. See main text for detailed description and **Fig. S19** for the structures of the dyes and FQs.

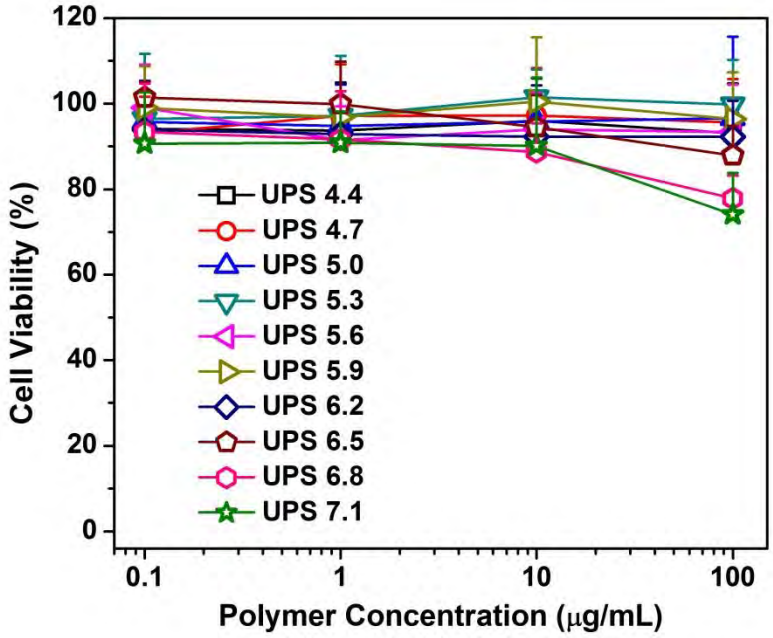

Figure S26. Evaluation of the cytotoxicity of UPS nanoprobes in H2009 lung cancer cells. H2009 cells were exposed to ten UPS nanoprobes with different pH_t for 4 hours at 37 ºC. The cell viability was evaluated by the MTT assay after 48 hours incubation. Error bars represent standard deviation of four replicate samples.